The Relationship Between Morphology and Mechanical Properties for Viscoelastic Polymer Composites

by

John J. Garvey

Washington & Lee University
Department of Physics and Engineering
Spring 1997

Introduction:

Advancement in the extrusion and molding techniques of polymers has spawned an increase in applications of polymeric materials. While previously polymers have been confined to nonstructural applications, development of new composites expands the use of polymers into the structural field. The scarcity of standardized mechanical properties for polymeric material imposes the need for standardized testing methods. For some applications, standardized testing methods have been developed, but continued investigation into this area is necessary.

The complexity of polymeric materials creates difficulty in the determination of mechanical properties. Temperature, time-dependence and effectiveness of reinforcing additives are a few characteristics that add to this difficulty.

Advanced extrusion techniques create the ability to mold polymer composites into profiles to be used commercially as railroad ties[1]. Investigation into the relationship between molecular, morphological and mechanical properties of this material is necessary to provide complete characterization of the material. Mechanical testing and Scanning Electron Microscopy are used in the following discussion to determine the validity of a method, extrapolating effects of sustained loading from short term tests for this material. If valid, this method may be used to determine the long-term effects of static loads on the material.

---

[1]Kenneth E. Van Ness, Thomas J. Nosker, Richard W. Renfree, Rashmi Sachan, Jennifer K. Lynch and John J. Garvey, *"Creep Behavior of Commercially Produced Plastic Lumber"*, Proceedings of Antec '97 (1997) #241

Polymers are molecules consisting of long chains of a repeating molecular unit known as a mer. A mer can be created by taking a molecule like ethylene or propylene and opening the double bond, creating a monomer with two or more bond surfaces. The number of primary bonds that a monomer can form, is called the functionality. As shown below, the opening of the double bond in the ethylene molecule creates a difunctional monomer.

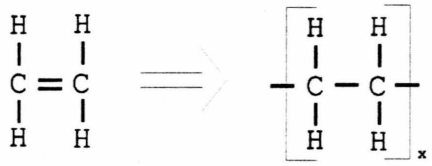

The degree of polymerization, x, for the polymer is the number of monomers making up the polymer.[2]

The functionality of a monomer is directly related to the structure of a polymer. The three main polymer structures are linear, branched and cross-linked. Difunctional monomers are confined to linear structure[3], in which the monomers are attached in a line (actually the shape is more of a zig-zag due to the bond angles in a tetrahedral molecular shape). Monomers of trifunctionality or greater can be branched, where smaller chains extend off a main chain, like branches from a tree trunk. Monomers with functionality of three or higher can also be cross-linked. In a cross-linked polymer, chains are connected three-dimensionally by shorter chains.

---

[2]Stephen L. Rosen, Fundamental Principles of Polymeric Materials (New York: John Wiley and Sons, Inc., 1993, pp. 13 - 18

[3]Difunctional mers may be used in the branches of a branched polymer, but not in the main backbone, or trunk.

The bonding between polymer chains is an essential characteristic in determining the relative strength for each type of polymer structure. The cross-linked polymer is generally the strongest structure because it is held together by primary covalent bonds in three dimensions. Linear and branched polymer chains are held together by weaker intermolecular forces, like van der Waals and hydrogen bonds. Linear and branched polymers often exhibit characteristics of flow at lower temperatures than cross-linked, because intermolecular forces are overcome with less energy. This is not the case for cross-linked polymers, because melting would require breaking primary bonds which requires high dissociation energy. Linear polymers can exist in crystalline or amorphous state. In a crystalline polymer, chains are organized in an ordered, close-packed arrangement, which governs their hard and brittle nature. Amorphous, non-crystalline polymers have disordered chains and are generally rubbery. There is no such thing as an entirely crystalline polymer, so all polymers have some amorphous material.[4]

The mechanical characteristics of a polymer are greatly dependent on its glass transition temperature, T_g. Below this temperature a material will exhibit hard and brittle characteristics. Above T_g, a material will be soft and rubbery and will exhibit characteristics of flow. The value of a material's T_g relative to its application temperature determines its usefulness. Different polymers have different glass transition temperatures, which is why polymers are used in

---

[4]Stephen L. Rosen, Fundamental Principles of Polymeric Materials (New York: John Wiley and Sons, Inc., 1993, p. 105

applications ranging from car tires, where a soft, rubbery material is needed, to structural applications where rigidity is necessary.

Since T_g can vary significantly from one polymer to another, it is useful to investigate the factors that affect T_g. Several factors affect the relative value of T_g, one of which is known as free volume. Free volume is defined as the difference between the volume occupied by the actual molecules, and the specific volume. If you were looking at a simple cubic unit cell for any molecule, the free volume would be the empty space within the cube. Greater free volume allows space for the molecules to move around, resulting in a lower glass transition temperature.

In addition to free volume, the attractive force between molecules affects T_g. If the attractive force is high, greater energy is necessary to cause movement of molecules, and, therefore, the glass transition temperature will be greater. The internal mobility and stiffness of chains impacts T_g. Since the backbone of a polymer consists of single carbon-carbon bonds, rotation about this bond can occur. Polymers with large bulky side groups will have higher T_g, due to steric hindrance. These side groups will increase the barrier to rotation so the chains will be less likely to slip by, therefore increasing T_g. The stiffness of a polymer chain's backbone will make coiling and uncoiling difficult, resulting in an increased T_g.

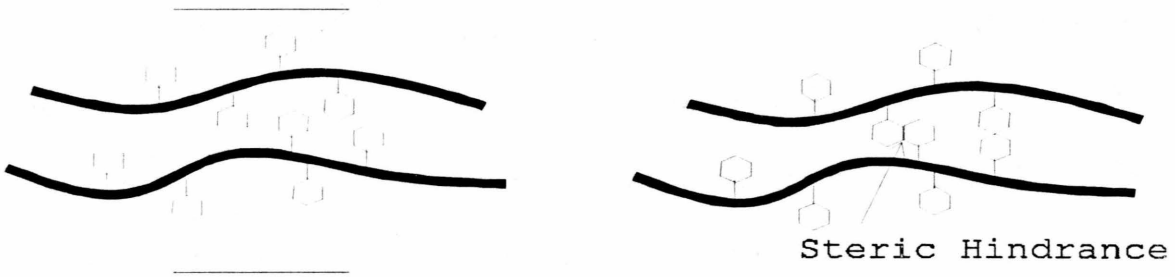

The chain length of a polymer will affect the value of the glass transition temperature. The relationship :

$$T_g = T_\gamma^\infty - \frac{C}{x}$$

where T_γ^∞ is the glass transition temperature for a hypothetical polymer with infinite molecular weight, C is constant for the polymer, and x is the degree of polymerization. As x approaches infinity, T_g approaches $_\gamma$, therefore, the longer the chain, the higher T_g. What actually is happening is that longer chains become more entangled, so the polymer will be stiffer.[5]

On the molecular level, four types of motion are characteristic of polymers. Vibration of atoms about their equilibrium positions is one type of motion which occurs constantly. This motion requires little energy and is known to occur in molecules other than polymers. Another type of motion occurs when a few atoms of a polymer (five or six) may move along the chain. When this motion occurs on a larger scale - motion of 40 to 50 atoms along the chain- it is described by the term cooperative wriggling. Coiling and uncoiling of polymer chains is also cooperative wriggling. The fourth type of molecular motion is the translational motion of entire molecules. In this type of motion entire chains slide past each other. This is the molecular representation of flow. Cooperative wriggling and translation of entire molecules require a greater amount of energy than the previous two types of molecular motion. These two types of

---

[5]Stephen L. Rosen, Fundamental Principles of Polymeric Materials (New York: John Wiley and Sons, Inc., 1993, pp.106 - 108

motion are considered "frozen out" below a molecule's glass transition temperature.[6]

Under stress chains may uncoil and slide past each other causing deflection in the material. When this occurs below T_g, the chains will act like a spring and pull itself back into place. This accounts for the elasticity of a polymer molecule. Under long periods of continued stress, the glass transition temperature may be affected so that the polymer chains do not spring back into place after deflecting. This type of deformation is called creep, and is the main focus of the analysis to follow.

Viscoelasticity:

Traditionally, materials can be placed in two different categories, elastic solids and viscous fluids. If the applied stress on a material is below the yield stress for that material, an elastic solid will deflect instantaneously, and then fully recover its original shape when the applied stress is removed. This behavior yields a linear relationship between stress and strain. A viscous fluid reacts in a similar manner, in that it enjoys a linear relationship between stress and the rate of strain. The following relationships govern stress and strain for a solid and fluid, respectively.

$$\sigma = E\epsilon \qquad\qquad \sigma = \nu\dot{\epsilon}$$

---

[6]Stephen L. Rosen, Fundamental Principles of Polymeric Materials (New York: John Wiley and Sons, Inc., 1993, pp.103 - 104

where sigma is stress, epsilon is strain, epsilon dot is the rate of strain, nu is viscosity and E is young's modulus. The above information governs most materials and allows the application of fairly simple predictive techniques. Polymers, however, fall in between the distinction of elastic solid and viscous fluid. This fact leads to complex relationships between stress and strain, and makes predictive techniques significantly more difficult.

Like many solids, polymers have crystalline molecular structure in addition to a portion of non-crystalline, or amorphous material. Since no polymer is 100% crystalline, the amorphous and crystalline portions of a polymer will contribute to its mechanical behavior. The magnitude of this contribution is dependent on the percentages of amorphous and crystalline material in the polymer. This provides another problem: How can one investigate mechanical properties of a polymer incorporating both viscous and elastic behavior?

Dynamic mechanical testing is one method of clarifying this problem. A sinusoidal strain rate is applied to a material while simultaneously measuring the stress response. For a linear elastic solid, the stress response will be in-phase with the applied strain. For a viscous material, the stress response will be 90 degrees out-of-phase due to the fact that stress is linearly related to the derivative of strain with respect to time.

$$\epsilon = \epsilon(t) = \epsilon \sin(\omega t) \qquad \dot{\epsilon}(t) = \dot{\epsilon} \cos(\omega t) = \dot{\epsilon} \sin(\omega t + \frac{\pi}{2})$$

For a linear elastic solid:

$$\sigma = \sigma' = E\epsilon \sin(\omega t)$$

where omega is the frequency of applied strain. For a viscous material:

$$\sigma = \sigma'' = \nu\,\omega\,\epsilon\cos(\omega t)$$

For a material that is a combination of viscous and solid material, the stress response can be converted into a stress vector, where the first term governs elastic behavior and the second governs fluid behavior.

$$\sigma = \sigma' + \sigma'' i$$

'i' is the out-of-phase unit vector. If a storage modulus and a loss modulus are defined: then a complex modulus can be defined as:

$$G_{storage} = \frac{\sigma'}{\epsilon} \qquad G_{loss} = \frac{\sigma''}{\epsilon}$$

$$G_{complex} = G_{storage} + G_{loss} i$$

and a loss tangent delta:

$$\tan\delta = \frac{\sigma''}{\sigma'} = \frac{G_{loss}}{G_{storage}}$$

Figures 1 and 2 are provided to show the relationship between loss tangent, storage modulus, and

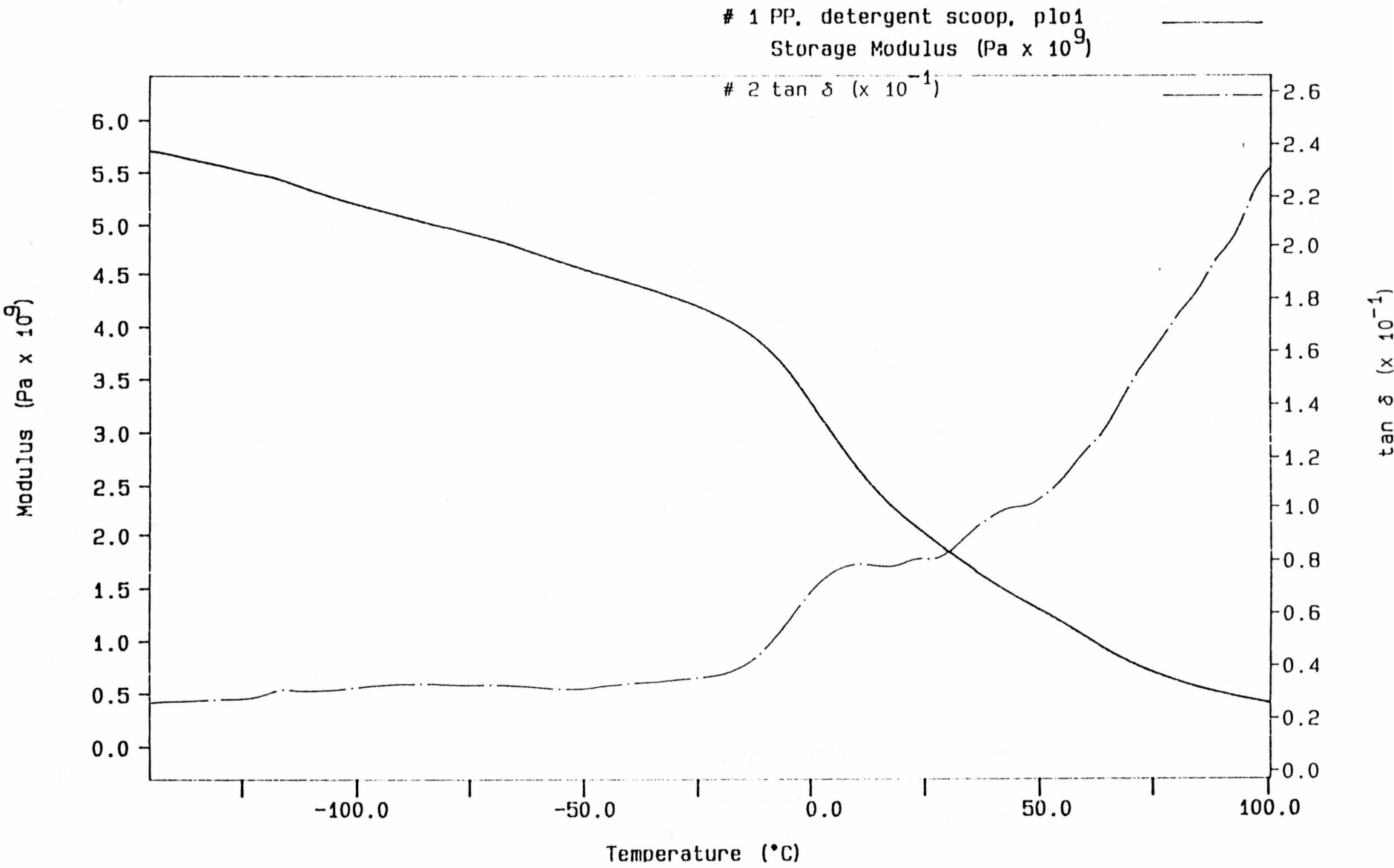

Figures 1 and 2 display the relationship between storage modulus and loss tangent as they vary with temperature.

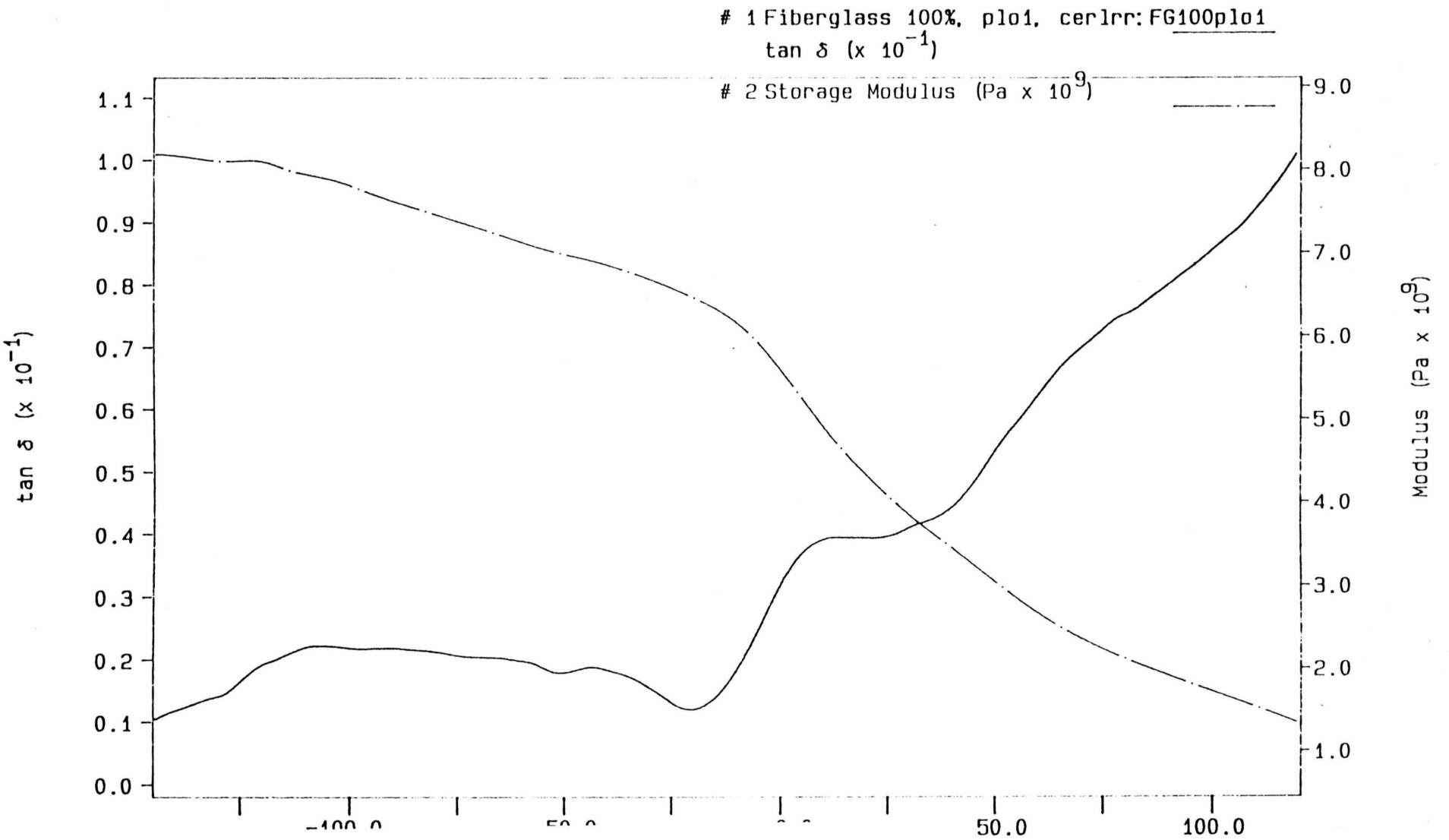
1 Fiberglass 100%, plo1, cerlrr: FG100plo1
tan δ (x 10^-1)
2 Storage Modulus (Pa x 10^9)
tan δ (x 10^-1)
Modulus (Pa x 10^9)
1.1
1.0
0.9
0.8
0.7
0.6
0.5
0.4
0.3
0.2
0.1
0.0
9.0
8.0
7.0
6.0
5.0
4.0
3.0
2.0
1.0
50.0
100.0

Figure 2

temperature for traditional polymers and polymer composites. Each plot relates storage modulus and loss tangent to temperature. Between zero and 50 degrees centigrade, the storage modulus displays a sharp decrease at the same time that the loss tangent displays a sharp increase. This phenomenon occurs at the glass transition temperature for the material in question. The material becomes increasingly amorphous until it reaches the glass transition temperature. Above this temperature, the polymer is completely amorphous, and displays fluid characteristics. The energy that was stored in the elastic portion is now "lost" or converted into heat. If more energy dissipates, a material will recover less, until finally no recovery occurs (fluid behavior).[7]

---

[7]Stephen L. Rosen, Fundamental Principles of Polymeric Materials (New York: John Wiley and Sons, Inc., 1993, pp. 321 - 326

Creep:

The relationships described above relate stress to instantaneous deformation of solids, or, if a stress is applied to a material, the material will yield in a short period of time. However, materials may continue to deflect under long periods of continuous loading. This phenomenon is known as creep. In everyday life, materials that have creeped are often described as "broken-in" or more drastically "worn-out." When one gets a new baseball glove, the leather is hard and tight. After repeated use the leather will permanently stretch and soften, or creep.

In polymers, creep is difficult to predict due to several factors, like the relationship between working temperature and glass transition temperature or rate of applied stress on a material. Creep in metals is often negligible due in part to the fact that the working temperature of metals is usually much lower than their melting points. In polymers, however, the difference between working temperature and glass transition temperature may be slight. Climate and seasonal temperatures may cause a polymer to reach its glass transition temperature. For metals, the rate of applied stress will not affect the modulus of elasticity, but in polymers stress rates have a significant effect on strain and modulus. When faster rates of stress are applied to polymers, at the same temperature, an increase in modulus is observed. In Figure 3, two stress-strain curves, A and B, are provided for a composite polymer. Two stress rates were applied to the same sample, where the stress rate on A was 500 times that of B. Curve A shows significantly less deformation at the same value of applied stress. The modulus varies for each curve; at the highest strain for B, the modulus for A is about 50% higher than that of B.

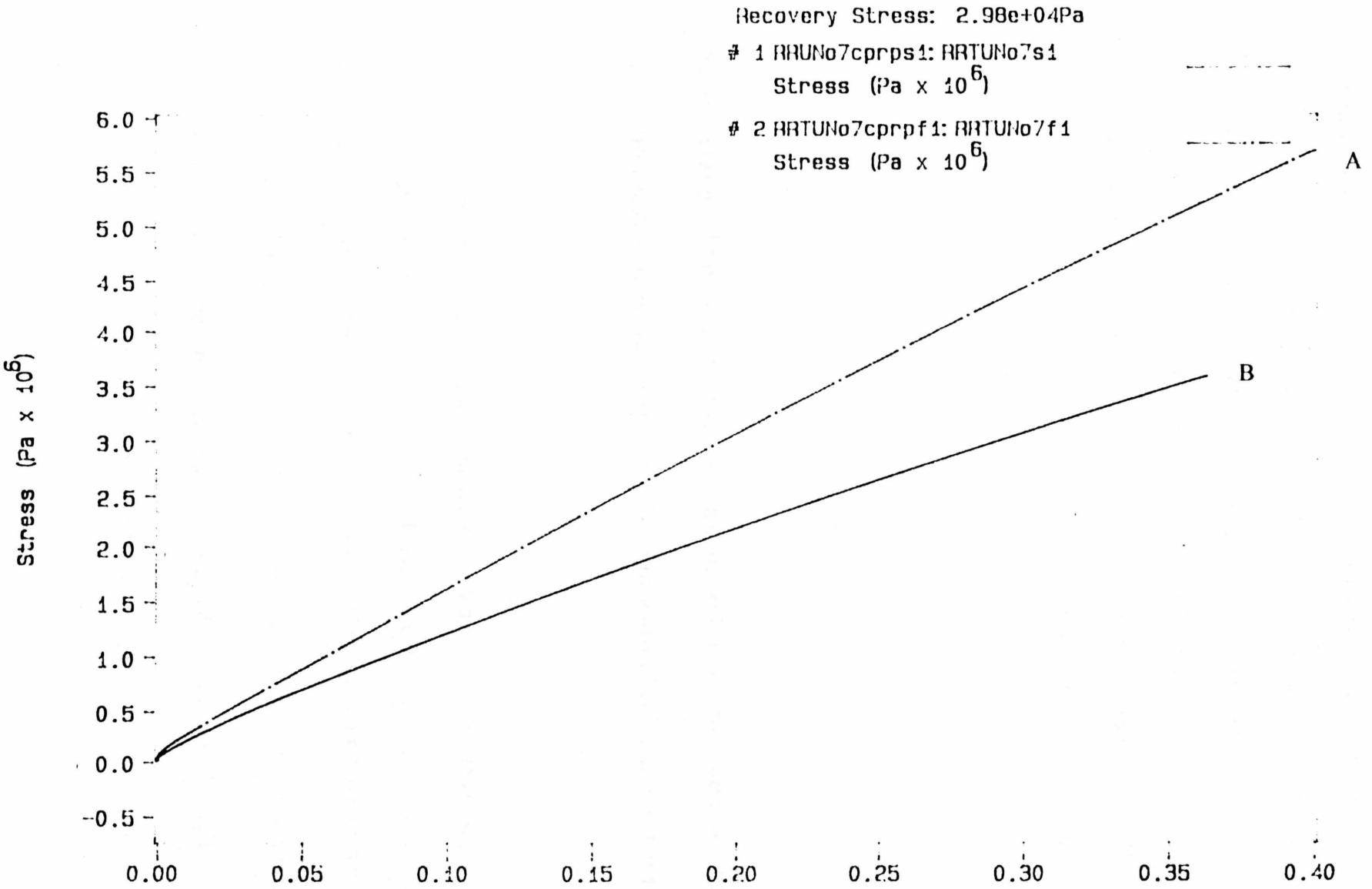

Figure 3 displays the effect of different stress rates on strain and modulus. The stress rate on curve A is 500 times that of B.

On a molecular level, deflection occurs in two different ways: 1) When bond angles in a molecule are stressed to rotate slightly; 2) When polymer chains are stressed to the point that they uncoil and slide past each other causing strain in the overall material. The first deflection mechanism occurs in most solids. The recovery of original bond angles explains elastic behavior in solids. The second mechanism is distinctive to polymers and may take longer to develop, adding to creep behavior in polymers.

The purpose of the following analysis is to determine long term creep values for the material in question using ramped values of stress and strain.

In order to approximate creep data from ramped data, a relationship between creep stress and ramped stress must be found. For a standard creep experiment, stress is held constant at $\sigma = \sigma_c$ for a period of time $t = t_c$ rendering a stress vs. time curve with the shape of figure 4. A ramped curve with a stress rate $\dot{\sigma}$ has a stress $\sigma = \sigma_r = \dot{\sigma} t_r$ at time $t = t_r$, and has the shape displayed in figure 5. The areas under each curve are equal to $\sigma_c t$ and $\sigma_r t/2$, respectively. Equating the areas under the creep strain curve and the ramped strain curve gives:

$$\sigma_c t_c = \sigma_r \frac{t_r}{2} \qquad (1)$$

If $t_c = t_r$, then the relationship between ramped stress and creep stress is:

$$\sigma_r = 2\sigma_c \qquad (2)$$

giving the required stress rate in terms of ramped data:

$$\dot{\sigma}_r = \frac{2\sigma_c}{t_c} \qquad (3)$$

With the ability to determine a stress rate that is related to creep stress, a method must be derived to create the long term ramp at the necessary rate using short term ramp data. In other words, we must find a relationship between different stress ramps.

In order to find a relationship between stress ramps, we attempt to find a point on one curve that has the same strain energy density ($\sigma\epsilon$) as a point on the other curves. The curves will be denoted as curve 2 and curve 1 with stress rates as $\dot{\sigma}_2$ and $\dot{\sigma}_1$ where $\dot{\sigma}_2 > \dot{\sigma}_1$. Pick a point on curve 1 and determine stress, strain and strain energy density (σ_1, ϵ_1, $\sigma_1\epsilon_1$). The next step is to find a point on curve 2 where $\sigma_1\epsilon_1 = \sigma_2\epsilon_2$. To accomplish this, find two values of $\sigma\epsilon$ on curve 2 which are the closest in value to $\sigma_1\epsilon_1$ (one higher and one lower than $\sigma_1\epsilon_1$). Call these values

$\sigma_a \epsilon_a$ and $\sigma_b \epsilon_b$ (Figure 6). To interpolate between $\sigma_a \epsilon_a$ and $\sigma_b \epsilon_b$, calculate the fraction ν, such that:

$$\sigma_2 = \sigma_a + \nu(\sigma_b - \sigma_a) \quad (4)$$
$$\epsilon_2 = \epsilon_a + \nu(\epsilon_b - \epsilon_a) \quad (5)$$

ν is defined:

$$\nu = \frac{-b + \sqrt{(b^2 - 4ac)}}{2a} \quad (6)$$

$$a = (\sigma_b - \sigma_a)(\epsilon_b - \epsilon_a) \quad (7)$$

$$b = \sigma_a(\epsilon_b - \epsilon_a) + \epsilon_a(\sigma_b - \sigma_a) \quad (8)$$

$$c = \sigma_a \epsilon_a - \sigma_1 \epsilon_1 \quad (9)$$

Once the above values are calculated, the exponent m can be calculated which satisfies the equation:

$$\frac{\sigma_2}{\sigma_1} = \left(\frac{\dot{\sigma}_2}{\dot{\sigma}_1}\right)^m \quad (10)$$

By repeating the previous steps for all points on curve 1, one can approximate curve 2 and determine m as a function of $\sigma\epsilon$. With the previous equation, stress values for any stress rate can be approximated, using data from a ramped experiment at another stress rate. Once the stress is calculated, strain can be determined by dividing $\sigma\epsilon$ by the corresponding value of stress. With

this method, one can determine long-term creep strains using data from short term stress ramps.[8]

[8]This method was created by Professor Ken Van Ness, and is yet to be published.

Scanning Electron Microscopy

In order to determine the relative strength of a composite, scanning electron microscopy(SEM) may be used. SEM allows one to observe the characteristics in the morphology of a material. The morphology can be defined as those characteristics which occur on a scale greater then the atomic level, but smaller than the macroscopic characteristics of the entire material. Morphological characteristics include the size and shape of additives and fillers, and their relationship to the substance to which they are added. The substance that occupies the major percentage of volume of the material will be referred to as the resin or matrix.[9]

---

[9]Linda C. Sawyer and David T. Grubb, Polymer Microscopy (New York: Chapman and Hall), 1987, p. 3 - 4

The polymer composite in question is a blended thermoplastic polymer reinforced with glass fibers. The matrix consists of polyethylene, with a polypropylene additive. The glass fibers were coated with polypropylene prior to the extrusion of the material. The mechanical properties of this composite will depend greatly upon the size, shape and distribution of the fibers, as well as the adhesion between the fiber and matrix.[10] The addition of polypropylene may strengthen the matrix if it mixes with homogeneity throughout the material.

Glass fibers will improve the strength and stiffness of the polymer. The degree of strength and the resistance to fatigue cracking will depend on the volume fraction of the fibers in the material. Adhesion between the fiber and matrix will determine whether the stress on the material is transmitted successfully from the matrix to the glass fibers (which are rigid and have a higher modulus). By observing the fracture surface of the material, one can determine the fracture mechanisms and, therefore, derive the relative strength of materials.[11]

SEM Sample Preparation:

The samples in question were prepared for SEM analysis in the following manner. The bulk material consists of a beam with a rectangular cross section with average dimensions of 23 cm x 18.5 cm. Beams of square cross sections with sides of 6 mm and lengths of 51 to 76 mm were taken from the bulk beam in two different directions. The first set of beams were taken longitudinally, or parallel to the flow direction and long axis of the bulk beam. The second set of

---

[10]Linda C. Sawyer and David T. Grubb, Polymer Microscopy (New York: Chapman and Hall), 1987, p. 11

[11]Linda C. Sawyer and David T. Grubb, Polymer Microscopy (New York: Chapman and Hall), 1987, p. 214 - 219

beams were taken from the bulk beam perpendicular to the flow and long axis of the bulk beam. These beams were notched so that a large crack could propagate until the beam fractured. These samples were secured at one end to create a cantilever and submerged into liquid nitrogen until an equilibrium temperature was reached (~ -195 C). A sharp force was applied at the crack, and the beams fractured into two pieces. These pieces were removed from the nitrogen and mounted onto a stub with a colloidal silver adhesive. Once dry, these samples were gold coated with the Pelco SC-4 Sputter Coater. These samples are now ready for SEM. The two directions will, from here out, be referred to as perpendicular, in which the flow direction is perpendicular to the plane of the SEM view, and parallel, in which the flow direction is in the plane of the SEM view. These samples were taken at various locations within the bulk beam, ranging from just below the outer surface of the bulk beam to a distance (or depth) of 63.5 mm below the surface of the bulk beam. Each SEM sample will denote a range of 6 mm from which the beam was taken out of the bulk beam. The above preparation methods were performed on materials classified as RRT28, RRT22, and RRTUN. The three materials contain the same ingredients, but were molded differently and/or possess different quantities of fibers and therefore different quantities of polymer. SEM figures will be characterized by material type, direction, and depth from which sample was extracted.

SEM Analysis

Sample 1: RRTUN

Scanning Electron Microscopy of this material at depths of up to 6 mm below the surface reveals consistent fiber behavior. The fibers are dispersed evenly throughout the polymer in both the perpendicular and parallel directions (SEM 1). There are few instances of clumps of fibers in

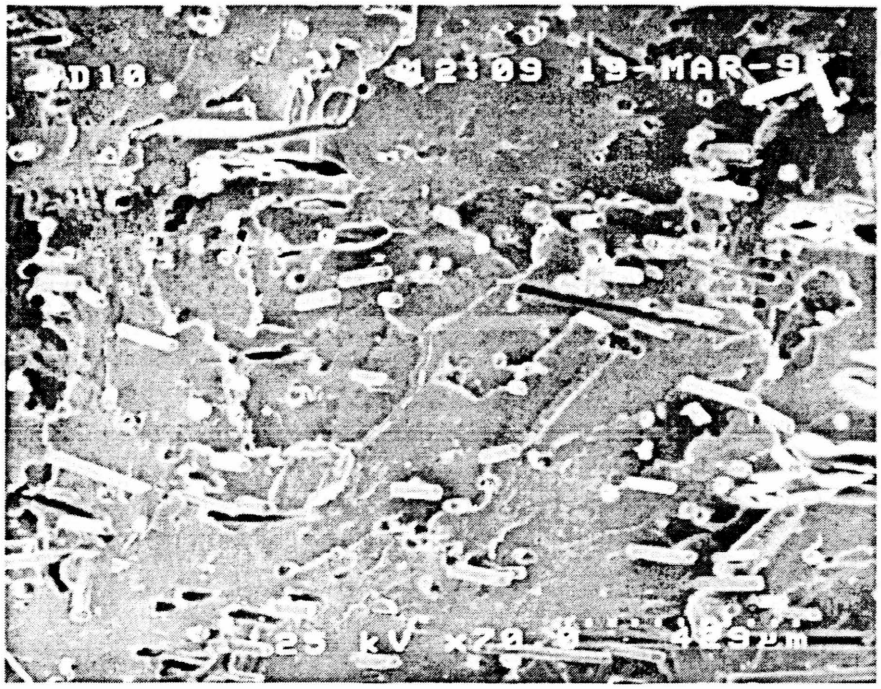

SEM 1 - RRTUN - Perpendicular - Near Surface - Overview of the matrix with fibers dispersed well throughout the matrix.

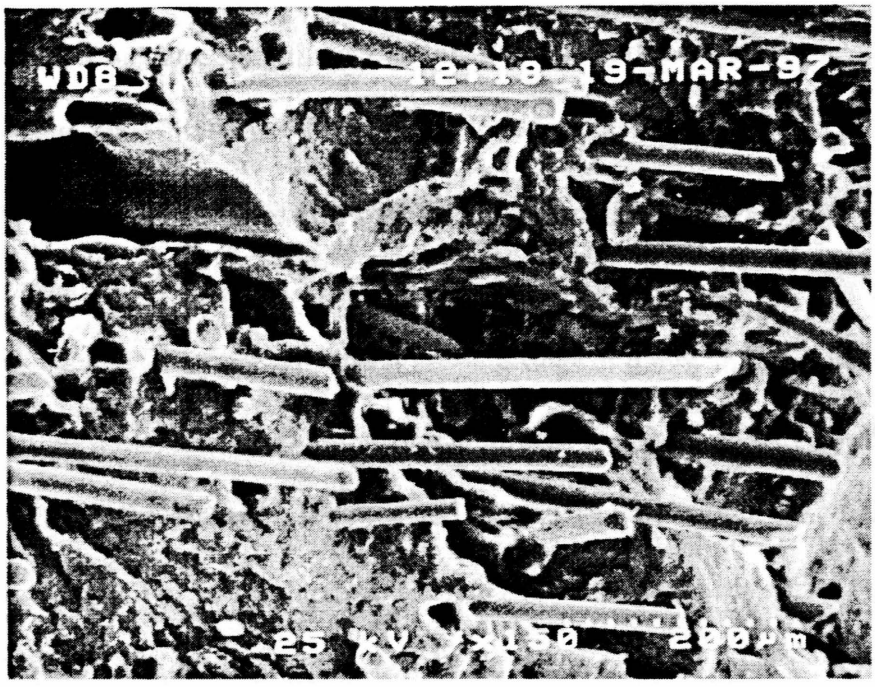

SEM 2- RRTUN - Paralell - Near Surface - Fibers are oriented in a uniform direction near the surface of the material.

the same area. The parallel and perpendicular directions display excellent fiber orientation with an obvious flow direction (SEM 2). This behavior is consistent for depths up to 19 mm below the surface. At this depth and below, the fiber orientation begins to break down as gaps and holes begin to appear in the actual matrix. These holes are small in size (about 150 microns) and do not occupy a significant percentage of the material's cross section until depths of about 38 mm. At greater depths, the flow directions are barely discernable and the holes are large enough to view with the naked eye (SEM 3).

At the surface, the perpendicular direction displays fibers, with the average fiber diameter of about 23 microns, protruding out from the polymer matrix. The parallel direction also shows long protruding fibers extending out of the matrix at lengths varying from 150 to 480 microns. SEM 4 and 5 are provided as examples for comparison of adhesive characteristics. SEM 4 shows an unknown composite in which the polymer adheres well to the glass fibers. The observer can see the large traces of polymer attached to the fiber. SEM 5 shows a polyethylene/fiber composite with poor adhesion between fiber and matrix. The protruding fibers are clean, and gaps exist between the fibers and the polymer matrix. Upon closer inspection (magnification of ~1000), adhesion between the fiber and matrix for the material in question is minimal. Some protruding fibers are whetted with minimal amounts of polymer, but most are clean (SEM 6). Lack of fiber/matrix adhesion is also indicated by the large holes left behind by fibers that have pulled out of the matrix (SEM 7, 8). In the perpendicular direction, gaps between the fiber and matrix occur at points where the fibers protrude from the matrix. Fiber/matrix adhesion improves slightly with increasing depth (SEM 9), but long, unwhetted, protruding fibers are dominant for this material.

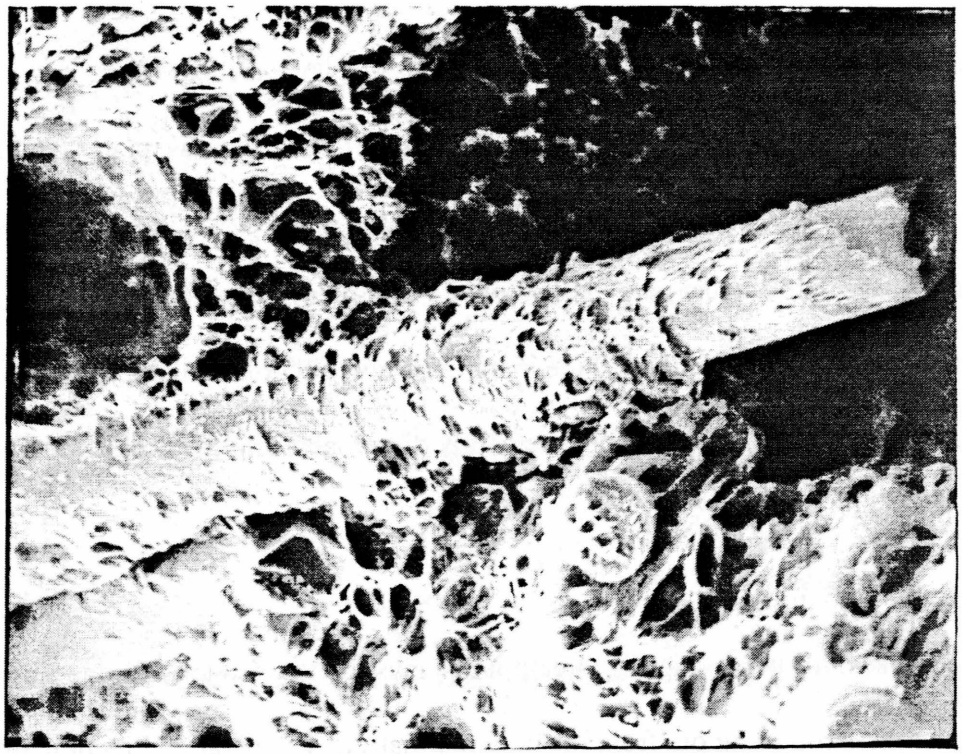

SEM 3 - This figure is provided for comparitive purposes as an example of an unknown glass fiber reinforced polymer with superior adhesive characteristics

SEM 4 - This figure is a high density polyethylene reinforced with glass fibers (no PP). It is provided for comparison of adhesive qualities

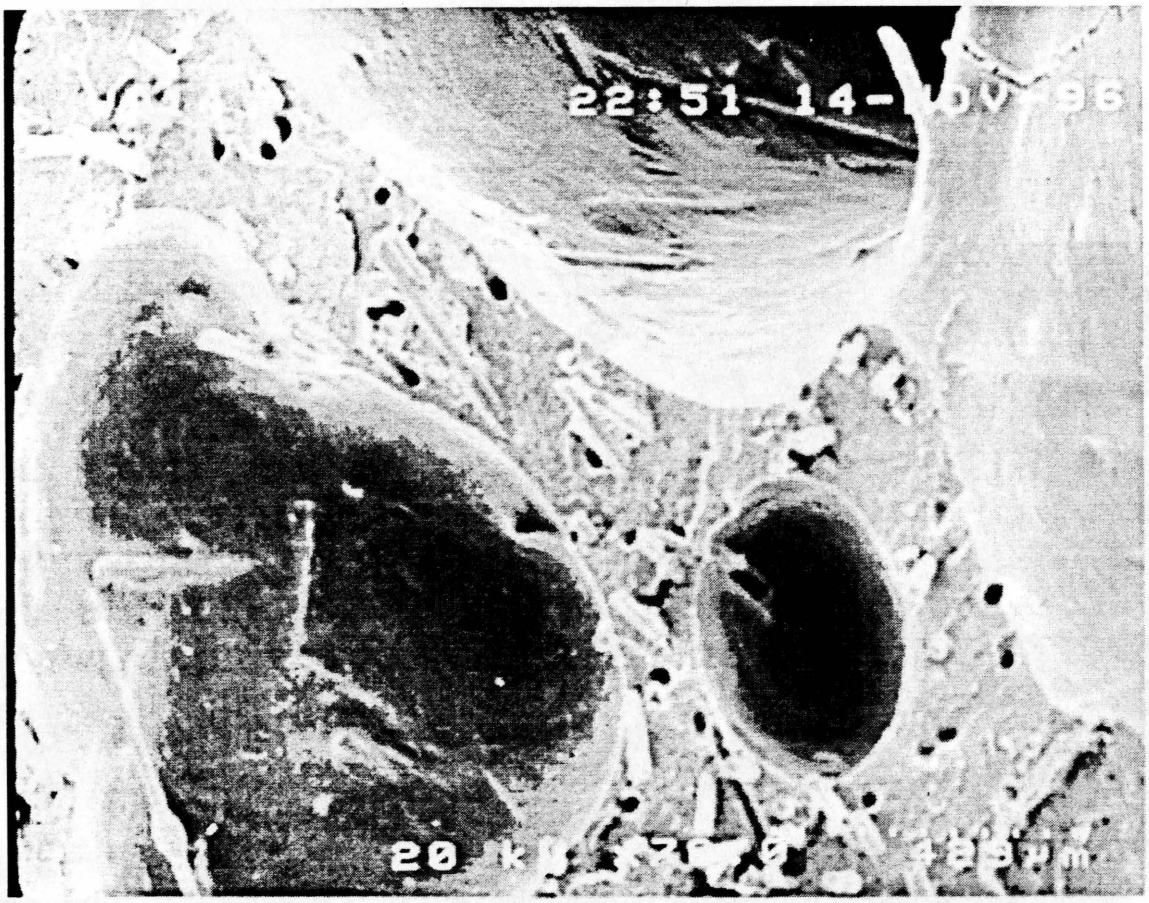

SEM 5- RRTUN- Perpendicular- 44 - 51 mm- Large holes occupy a large percentage of the cross section, and disrupt the orientation of glass fibers.

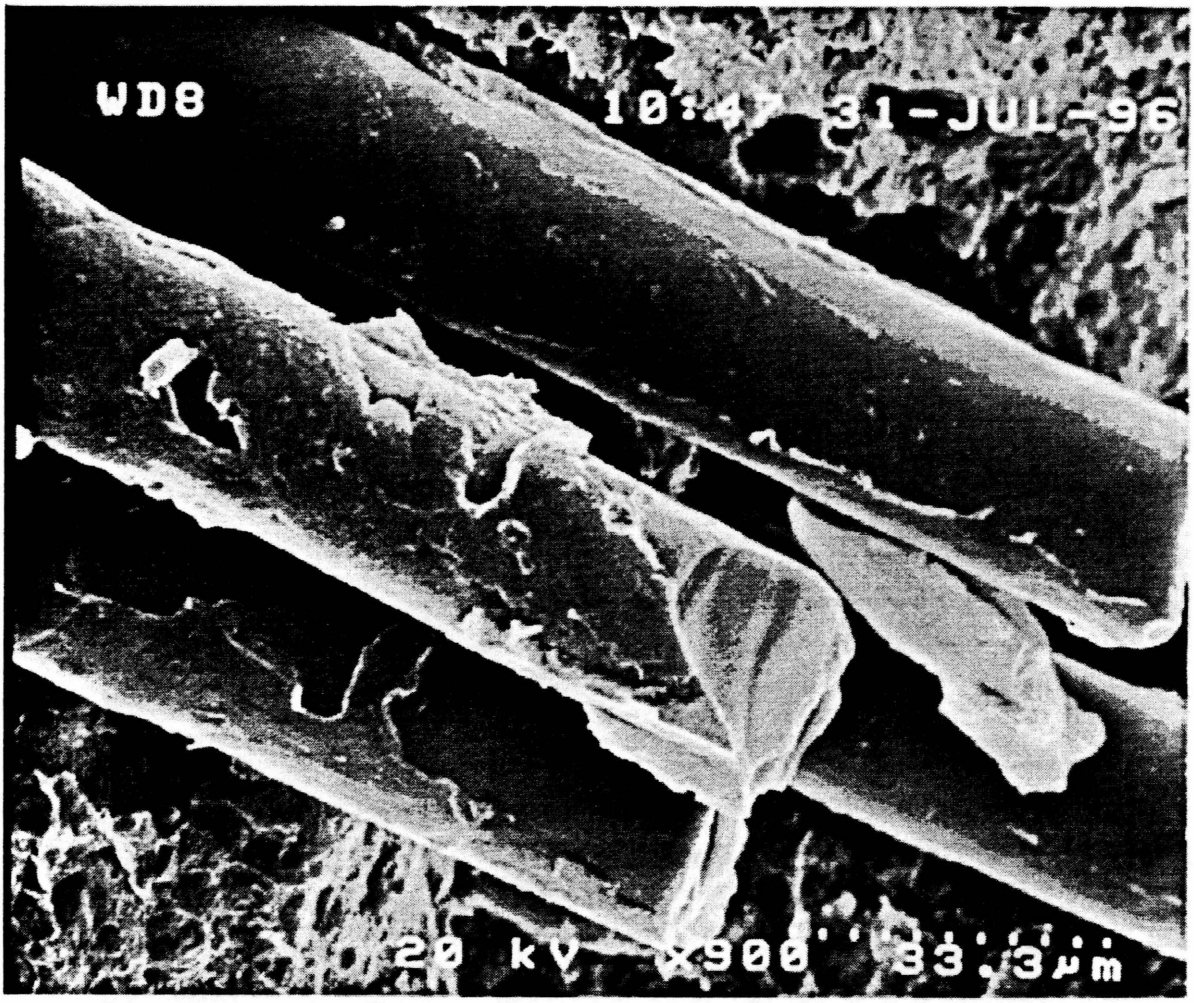

SEM 6-RRTUN- Parallel- 12.4 - 18.6 mm - Glass fibers protruding out of the matrix with minimal occurrence of polymer adhesion.

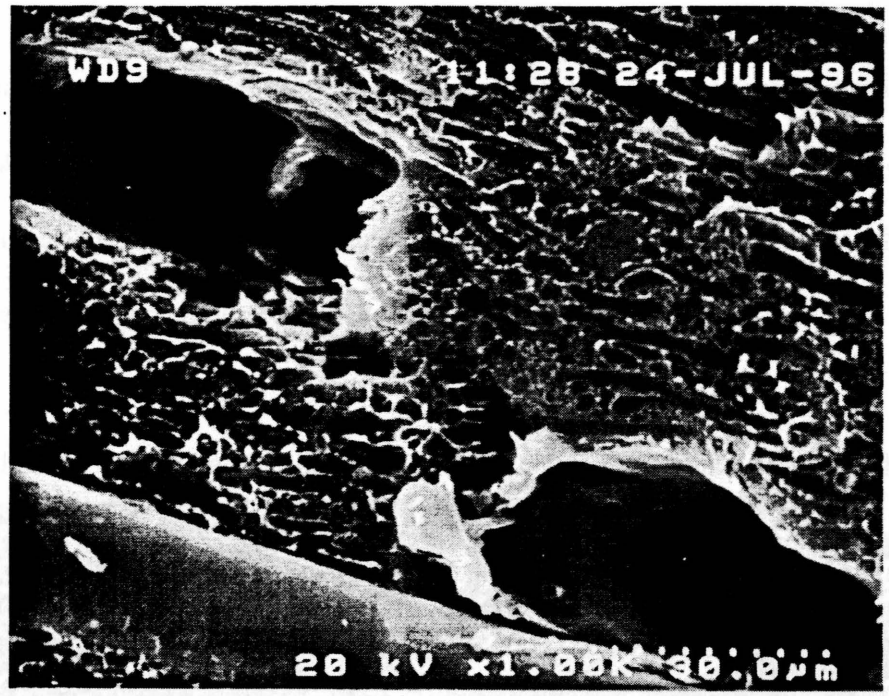

SEM 7 - RRTUN- Parallel- Surface- Holes where glass fibers have pulled out of the matrix. Dispersed phase appears as elliptical streams.

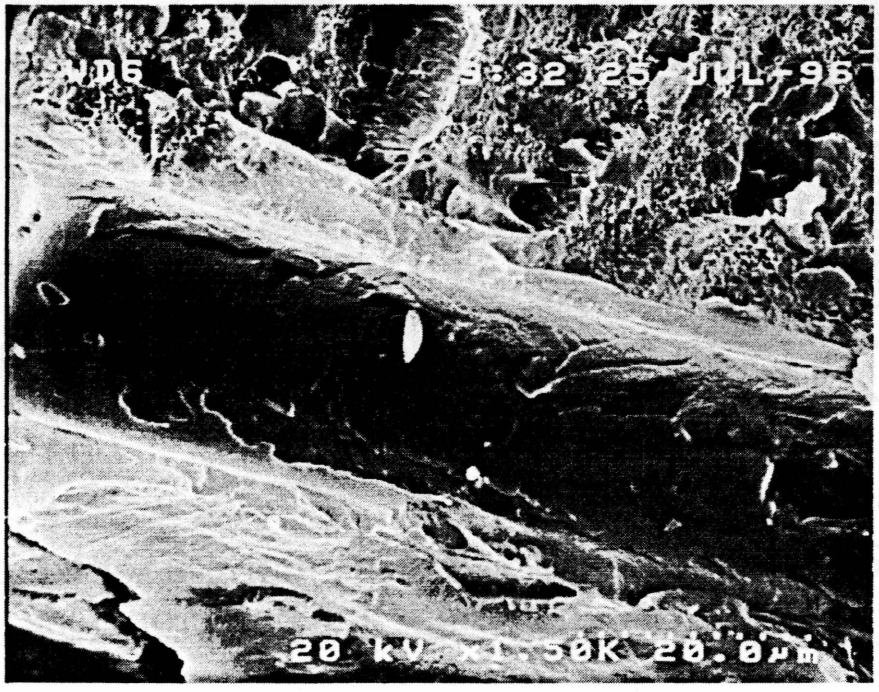

SEM 8 - RRTUN- Parallel- Surface- Channel where a glass fiber has pulled out of the matrix.

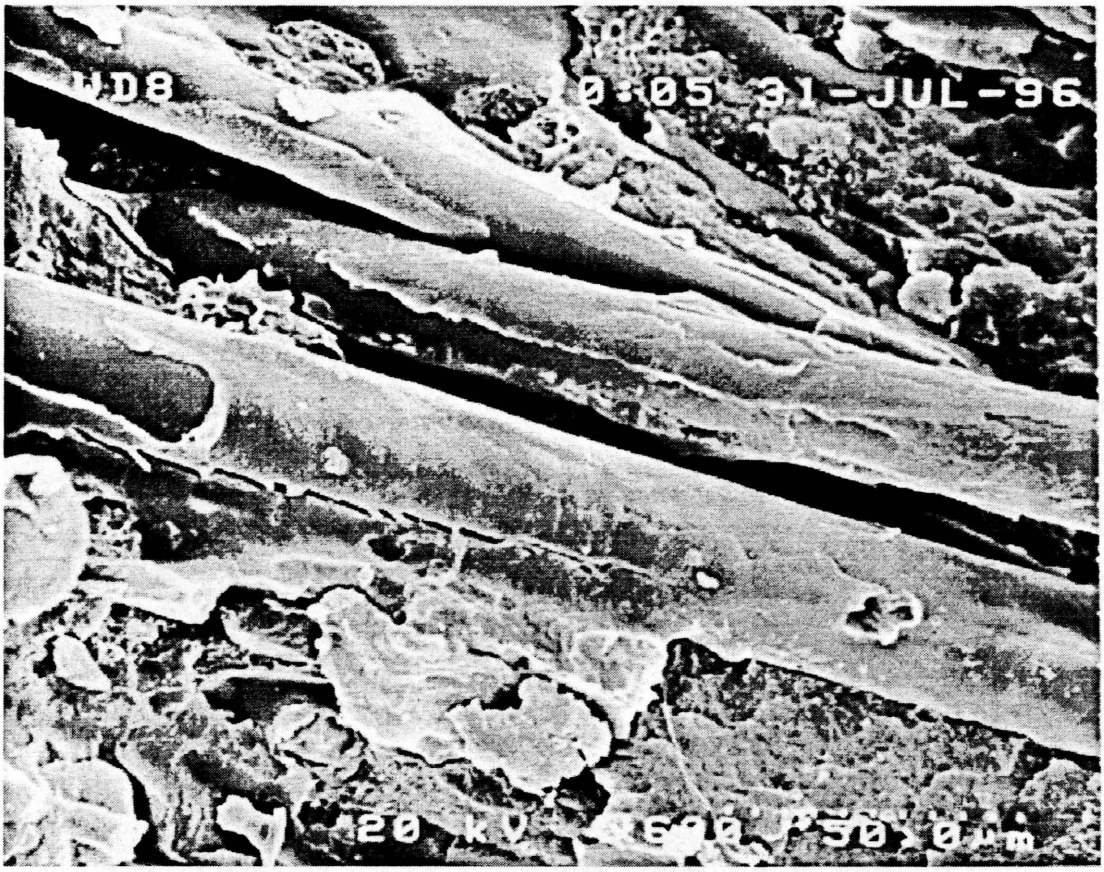

SEM 9 - RRTUN - Parallel- 6.2 - 12.4 mm- Minor adhesive charactaristics between glass fibers and polypropylene.

The matrix morphology at high magnification displays the relationship between polyethylene and polypropylene. Polypropylene occupies a smaller fraction of the entire material than polyethylene. PP forms different shapes within PE and will be referred to as the dispersed phase, because it is dispersed nonhomogeneously throughout the material.

Polyethylene takes on a web-like shape with the dispersed phase polypropylene occupying the gaps in the web (SEM 10). Near the surface, in the perpendicular direction, the dispersed phase often is of circular shape. At certain areas, the dispersed phase has similar radii and is settled within the gaps in the PE web. Although this shape is consistent at low depths, the size of dispersed phases is not. Large circular and elliptical phases are common and occur randomly throughout the matrix (SEM 11). The parallel direction typically displays an oblong, elliptical, dispersed phase (SEM 7, 12). This suggests that the dispersed phase is drawn in the flow direction into tube-like shapes. The dispersed phase is slightly more prevalent near glass fibers. Intense magnification of some holes and canals where fibers pulled out, reveals encasement of these fibers in PP (SEM 13). In all cases, a definite border between polyethylene and polypropylene is evident, suggesting that the two polymers do not mix well. Even when the dispersed phase occupies gaps in the web-like structure, definite borders between phases are obvious.

In addition to the sample fractured in liquid nitrogen, a sample fractured under mechanical testing at a temperature of 23 degrees C was prepared for SEM. The fracture surface is perpendicular to the flow direction. Microscopy of this surface supports some of the previous statements related to the fracture mechanics. Long protruding unwhetted fibers extend out of the

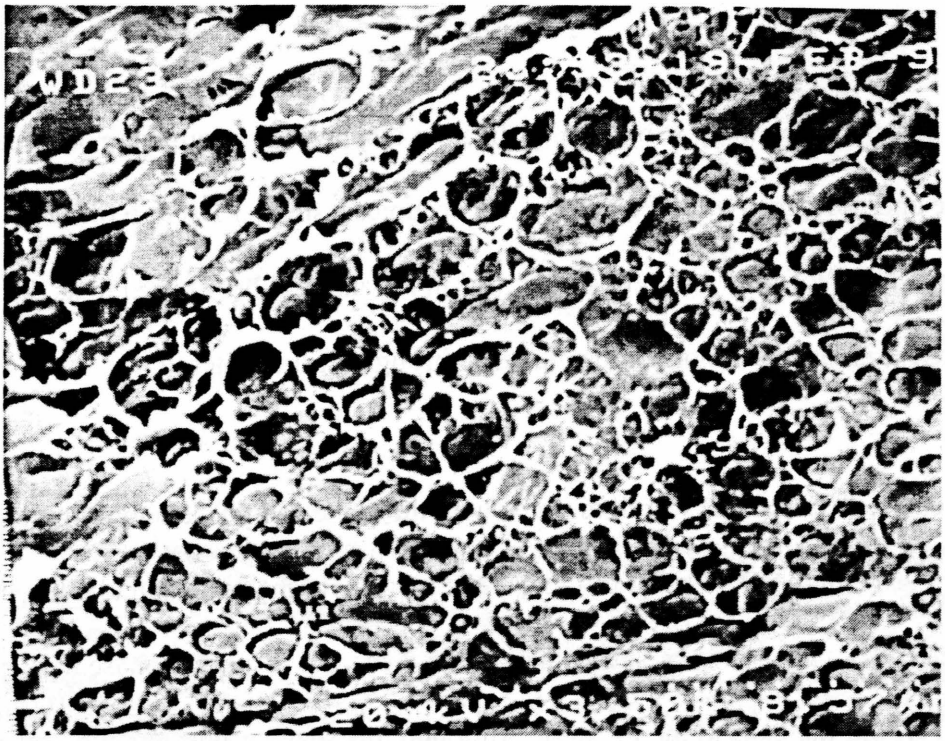

SEM 10 - RRTUN - Perpendicular- Surface- High magnification of matrix with dispersed phase PP filling the gaps within the web shaped PE.

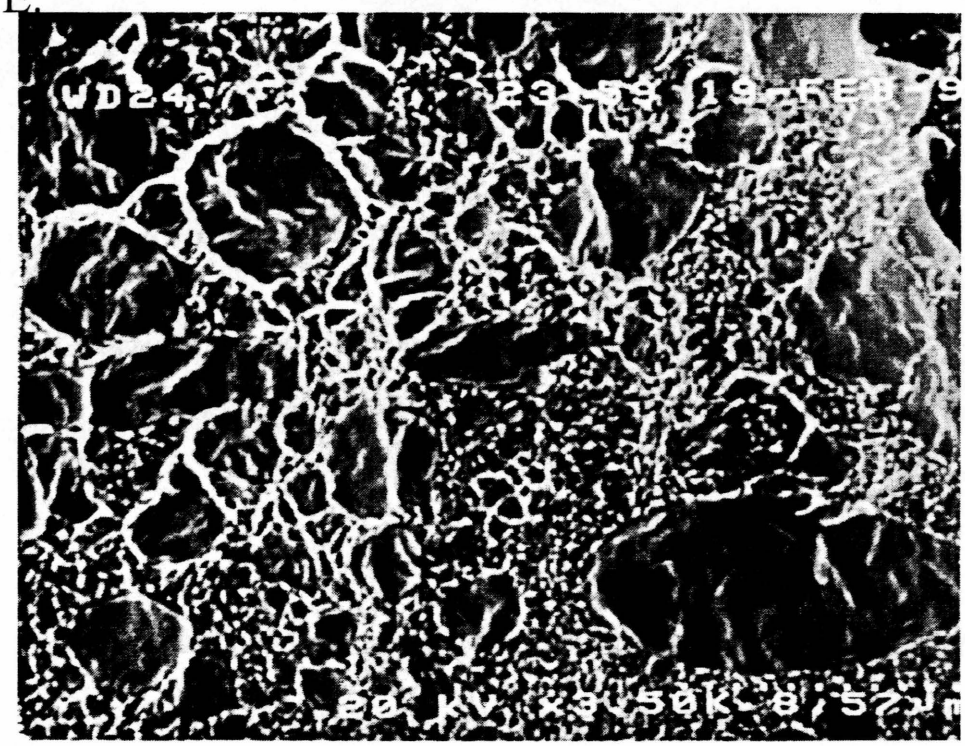

SEM 11 - RRTUN - Perpendicular- Surface- High magnificaiton of matrix with large dispersed phase occurring randomly throughout matrix

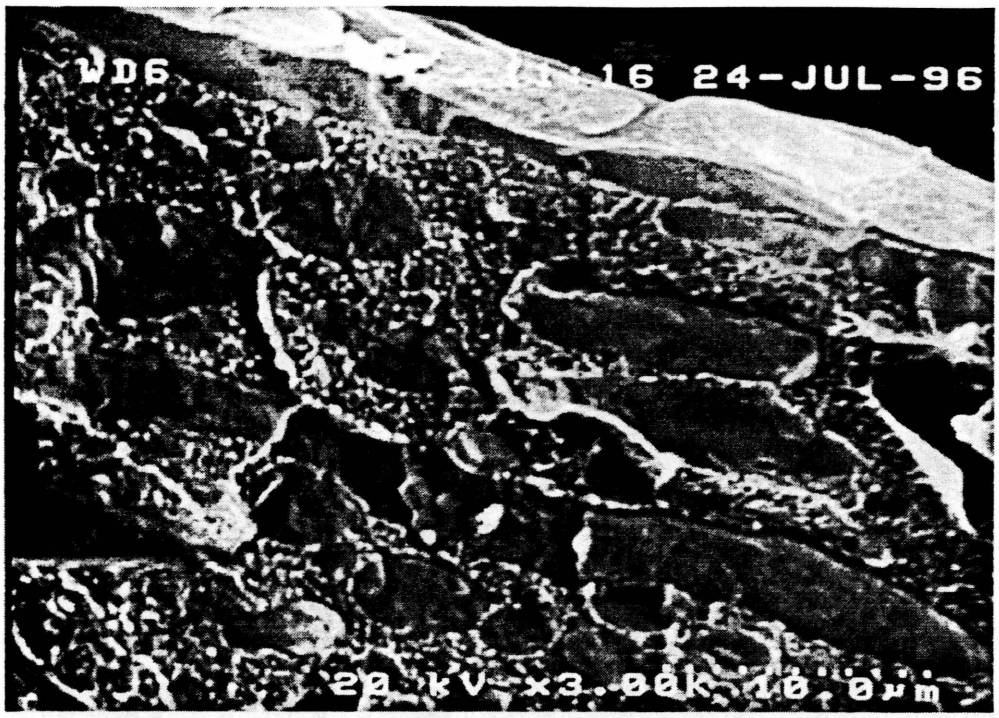

SEM 12 - RRTUN -Parallel- Surface- High magnificaiton of matrix near fiber channel. Dispersed phase is elongated in the direction of flow and is abundant near fiber channel. (Note: fiber channel is the dark space at the top right of the photo.

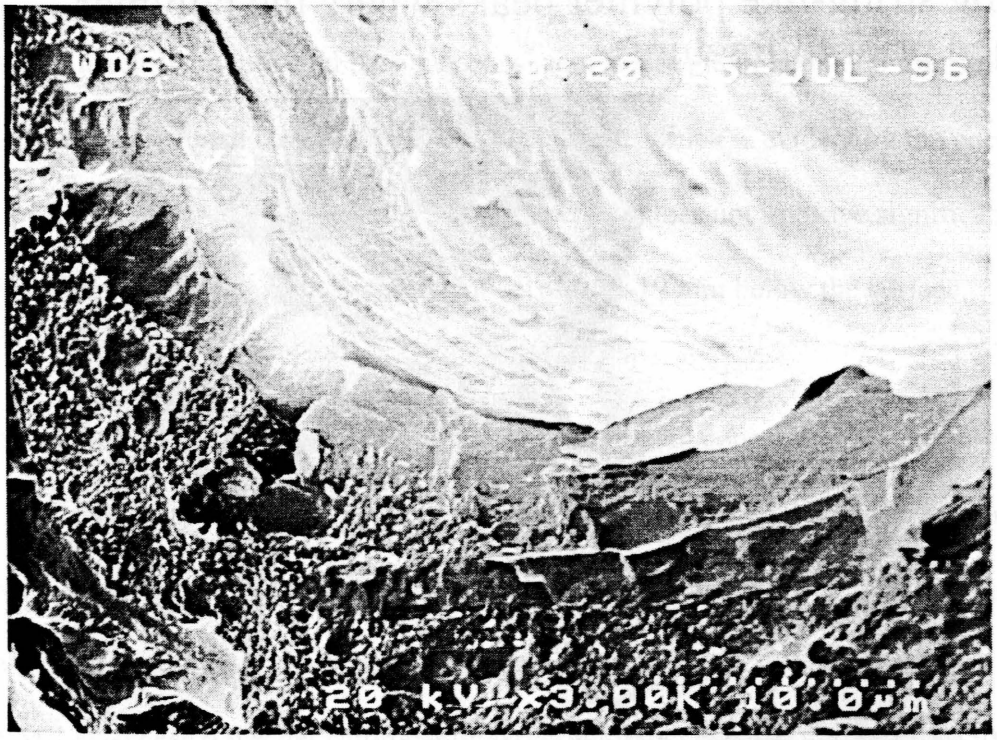

SEM 13 - RRTUN - Perpendicular - Surface- High magnificaiton of glass fiber protruding out of the matrix. The smooth PP almost forms a circle around the base of the fiber.

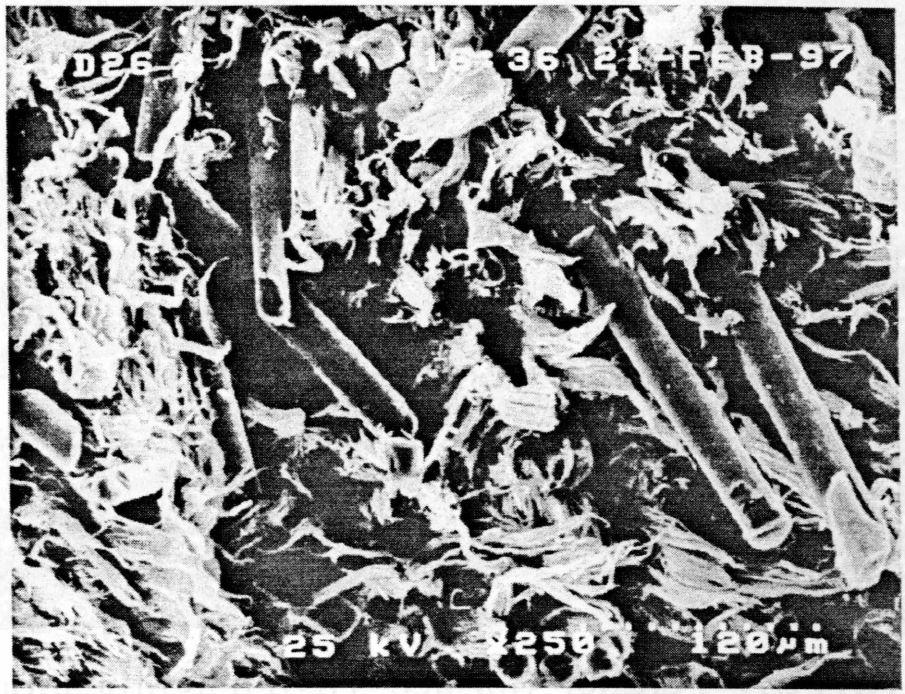

SEM 14 - RRTUN - Perpendicular - Fractured under mechanical testing at 23 C. Unwhetted fibers protruding out of the matrix with long string-like polymer peaks where the polymer deformed prior to fracture.

SEM 15 - Perpendicular - Fractured under mechanical testing at 23 C. High magnification of fiber/matrix relationship reveals gaps where polymer yielded under stress applied by fibers

matrix. The matrix consists of long string-like peaks that appear to have deformed plastically prior to failure (SEM 14). Near the base of fiber and matrix, large gaps between the glass fibers and polymer matrix exist. The polymer surrounding glass fibers yielded under stress applied by the fibers, causing large gaps between the fibers and matrix (SEM 15). Even at high magnification, different phases of polymer are not discernable.

Sample 2: RRT28

This material has similar morphological properties, and can hardly be distinguished from RRTUN. However, there are certain subtle but significant differences that may alter the relative strength of the material. Near the surface of this material (~0 - 3 mm), the orientation of glass fibers in both parallel and perpendicular views is poor. The fibers are directed in random directions, and the flow direction is indistinguishable (SEM 16A, 16B). Orientation gradually improves with increasing depth, and becomes consistent at a depth of about 2.5 mm below the surface. Dispersion of fibers is also poor at shallow depths, which is evident by the occurrence of clumps of fibers gathered in some areas. This dispersion does not improve significantly until 6 mm. Glass fiber dispersion is most consistent between 6-19 mm below the surface.

The morphological characteristics within RRT28 remain constant until a depth of about 12.7 mm, where voids in the matrix begin to appear. These voids are elliptical in the parallel direction with the long axis of the hole parallel to the flow direction. At this depth range(13 - 19 mm) the holes have lengths of about 300 microns and do not occupy a large percentage of the matrix (SEM 17). These holes get significantly larger with increasing depth - 400 to 500 microns at 19 to 32 mm (SEM 18). At this depth, fiber orientation begins to break down, with the holes

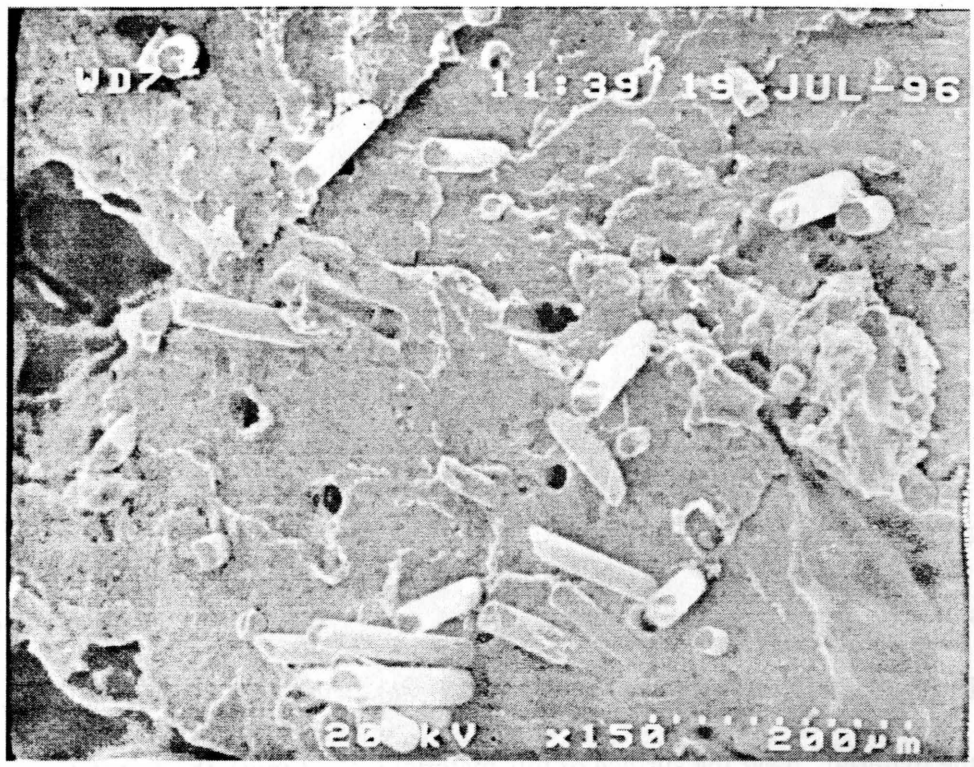

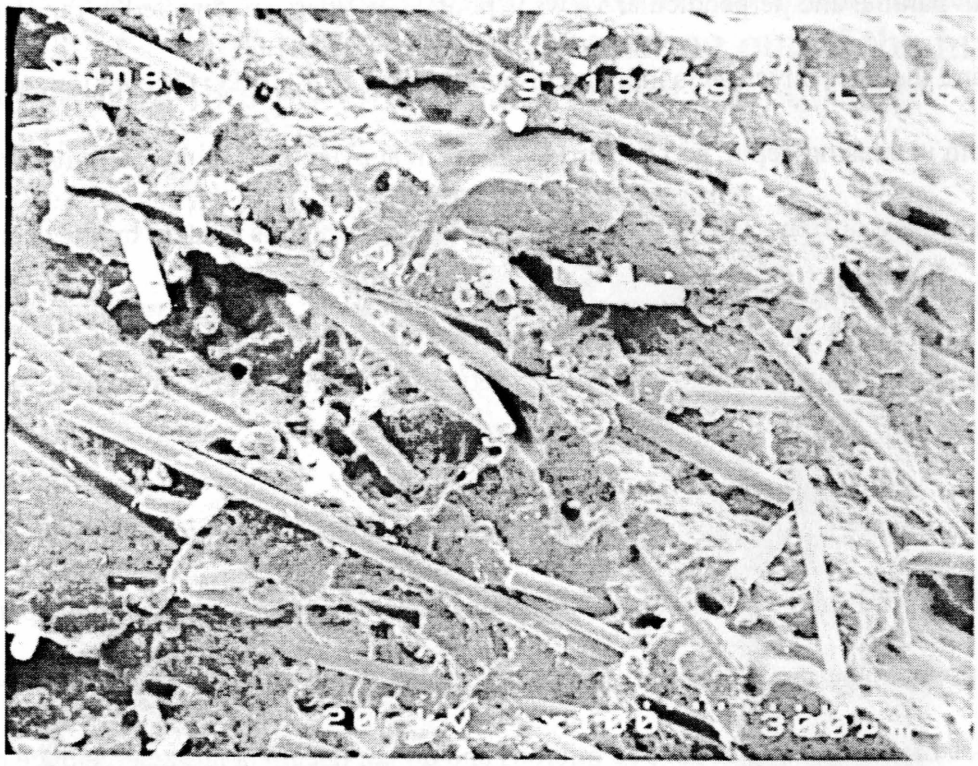

SEM16A(top) & 16B - RRT28 - Perpendicular and Parallel -Surface - Fibers extending out of the matrix display poor dispersion near the materials surface, evident by clumps of fibers in some areas. Poor fiber orientaiton in both directions displayed by randomness of fiber directions.

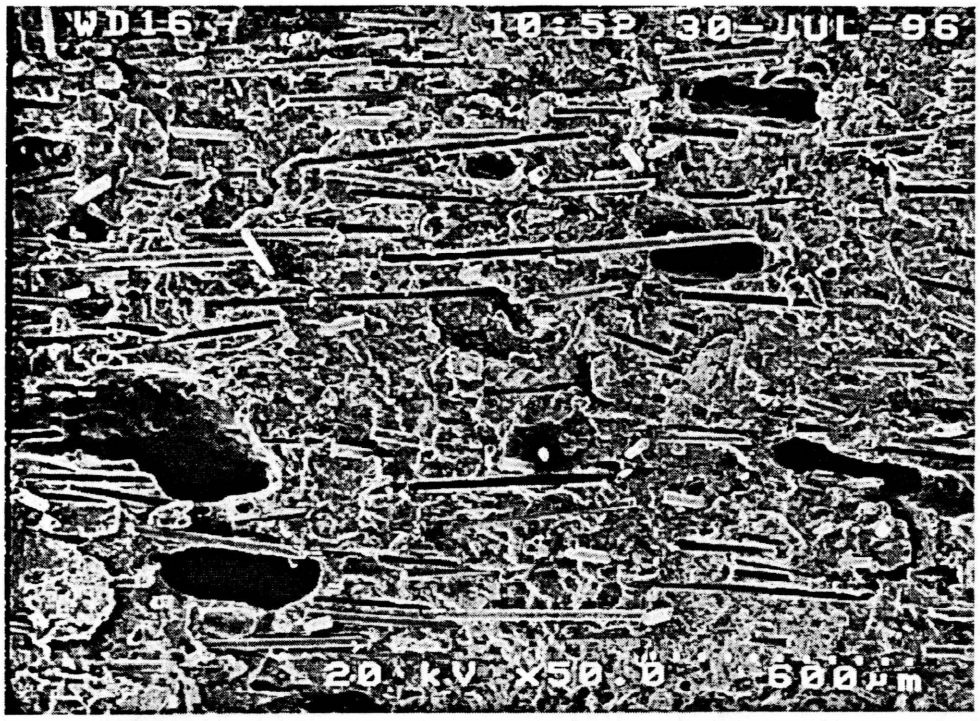

SEM 17 - RRT28 - .12.4 - 18.6 mm - Holes begin to appear at this depth, but do not interfere with fiber behavior. Orientation and dispersion of glass fibers display an obvious flow direction.

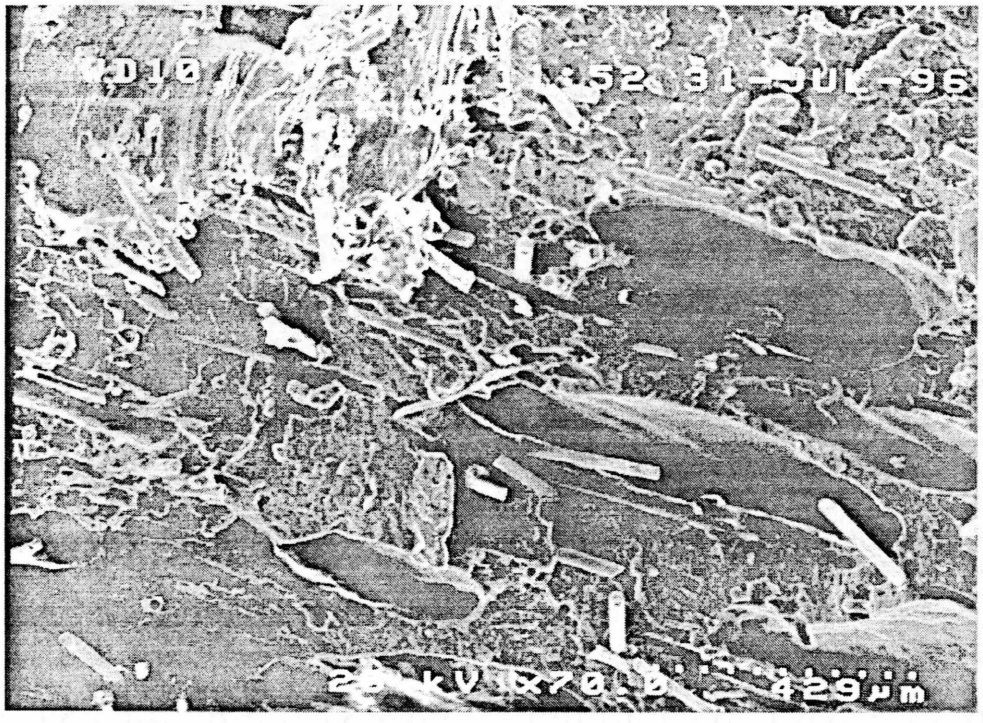

SEM 18 - RRT28 - 18.6 - 25.4 mm- Holes become larger (~500 microns) and the orientation of fibers begins to break down.

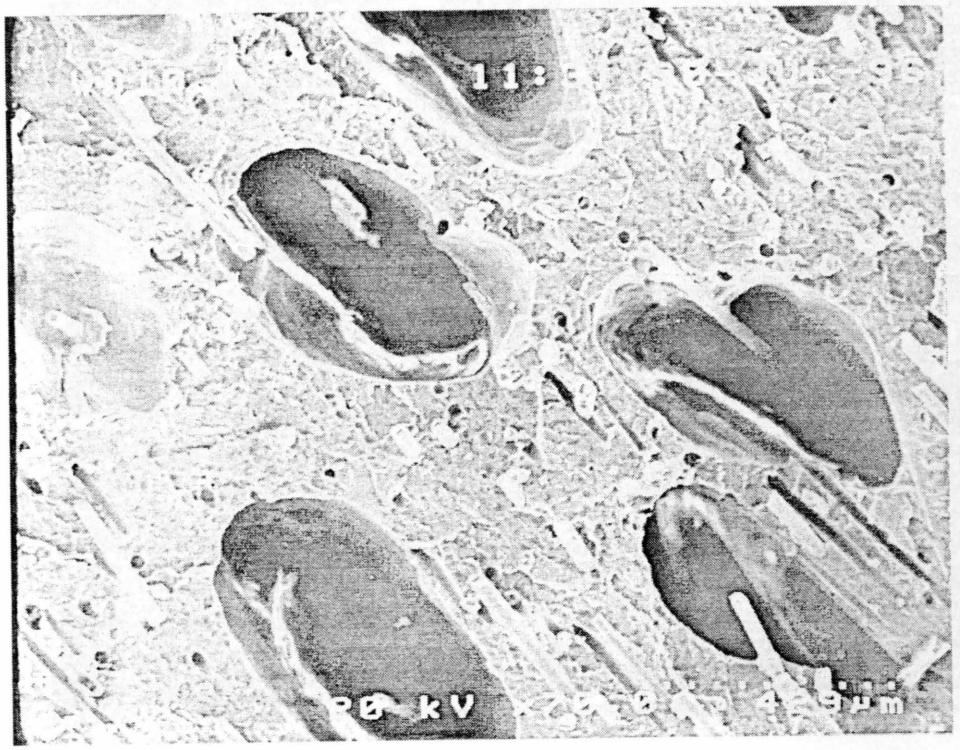

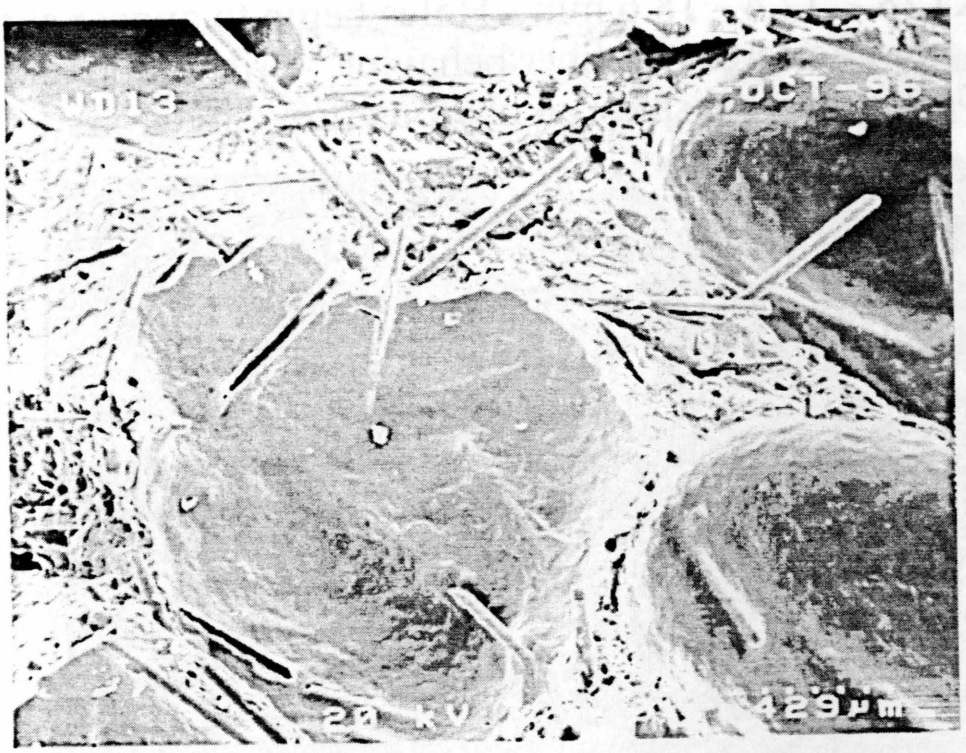

SEM 19 & 20 - RRT28 - Parallel - 25.4 - 31.6 mm, 44 - 51 mm -Holes become larger with increasing depth until they occupy most of the cross-section. No consistent fiber direction.

occupying a significant portion of the cross section (SEM 19). Below 44 mm, holes occupy most of the cross section with diameters in excess of 800 microns. No consistent fiber orientation or flow direction can be seen (SEM 20).

As in the case for RRTUN, RRT28 displays long clean glass fibers protruding out from the surrounding matrix. Near the surface there is little evidence of any polymer attached to the fiber ends (SEM 21). At increased depths, the adhesion between fiber and polymer improves slightly. This adhesion only occurs between fibers and polypropylene (SEM 22). Polyethylene does not adhere at all. In areas where polypropylene is more abundant, adhesion to the fibers occurs. At times PP encases the fibers (SEM 23).

The matrix morphology of RRT28 is significantly different from that of RRTUN. The web-like shape of polyethylene interspersed with a dispersed phase polymer is not evident here. The dispersed phase occurs in greater amounts and does not interact with PE (SEM 24). There are definite borders between the two polymers (SEM 25).

Sample 3: RRT22

RRT22 enjoys morphological characteristics that are nearly identical to those of RRT28. Poor orientation and dispersion of glass fibers is evident near the surface of the material. The fibers extend out of the matrix in different directions and flow direction is barely distinguishable. The orientation and dispersion characteristics improve and flow direction becomes obvious at a depth of about 6 mm (SEM 26, 27). These characteristics remain constant until about 19 mm below the surface. At a depth of 13 mm, holes in the matrix begin to appear, which are about 150 microns in diameter and do not occupy a large portion of the cross section. These holes increase in size with depth and interfere with fiber direction at 19 mm below the surface (SEM

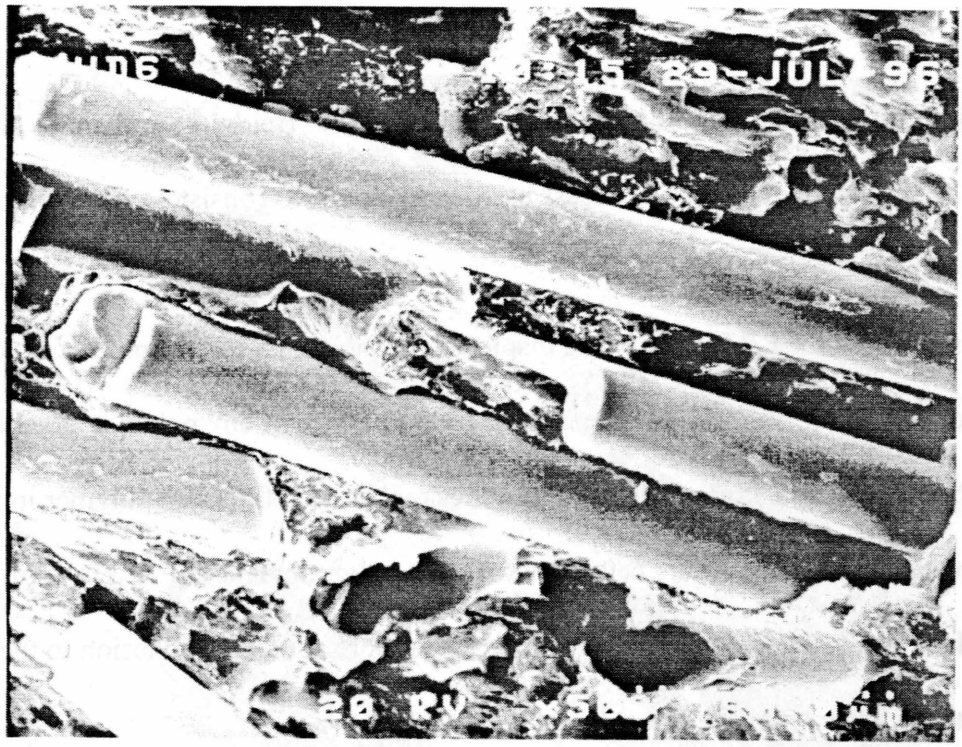

SEM 21 - RRT28 - Surface - Fiber ends protrude from the matrix with no polymer adhesion.

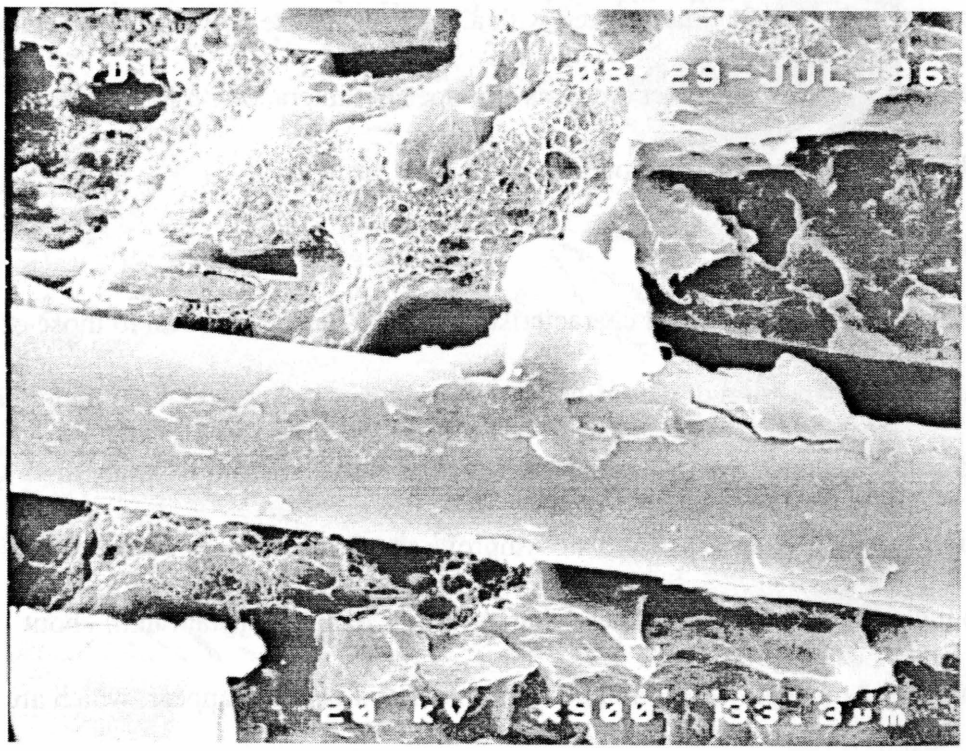

SEM 22 - RRT28 - Parallel - 6.2 - 12.4 mm - There is slight adhesion between Polypropylene and fibers. This adhesion has little effct in strengthening the material

SEM 23 - RRT28 - Surface - High magnification of a hole where a glass fiber has pulled out reveals PP existing as a border around the fiber.

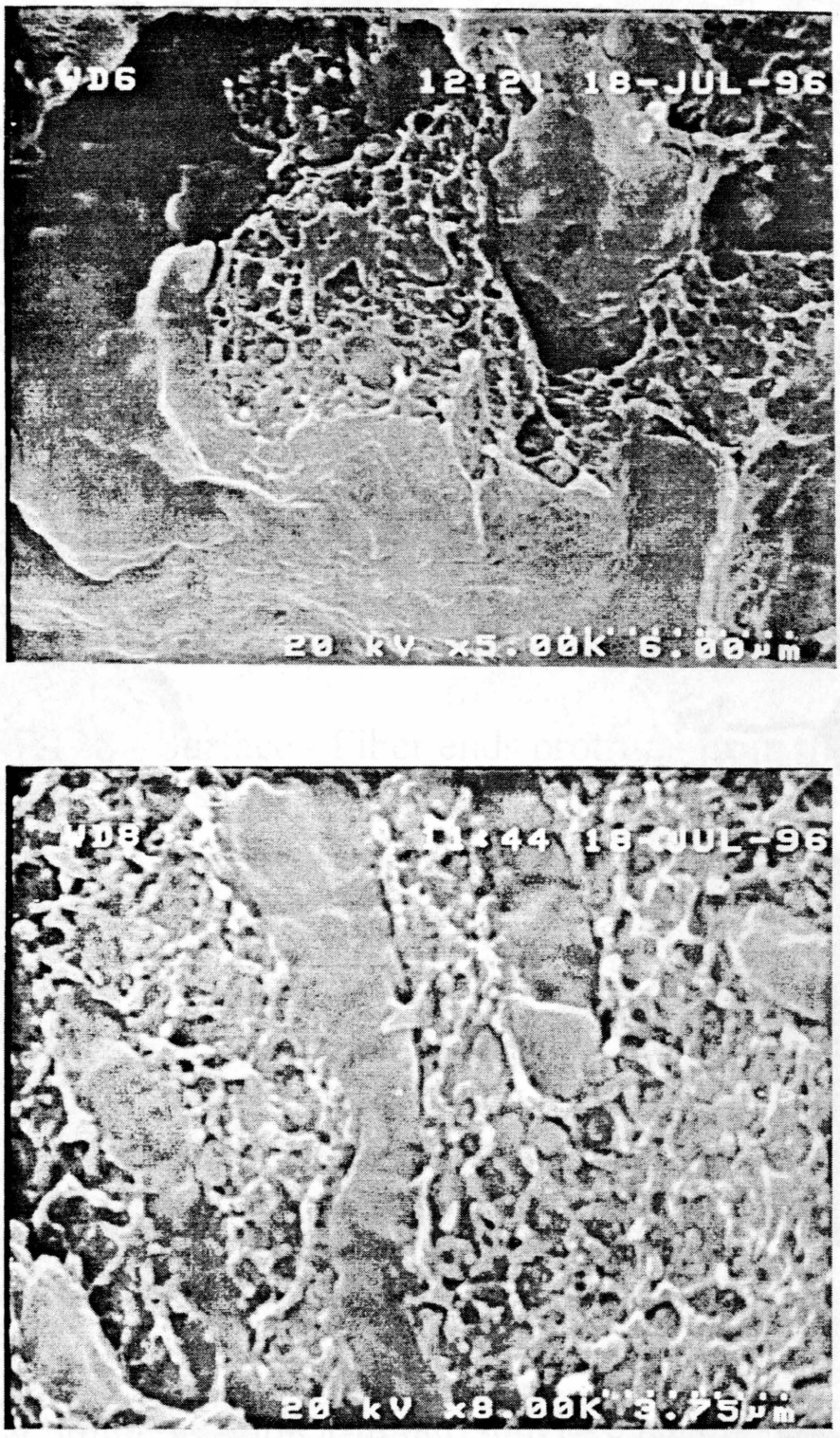

SEM 24 & 25 - RRT28 - Parallel (top) & Perpendicular - Surface - High magnification of matrix reveals PP in greater abundance in RRT28 than in RRTUN. The two phases of polymer are isolated from each other with a definite border between phases.

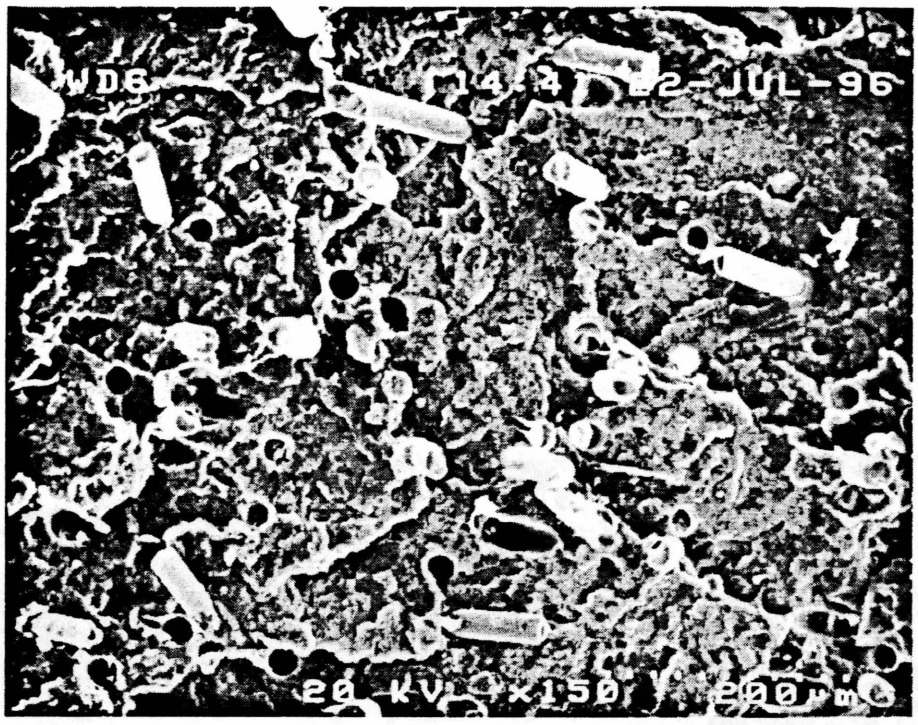

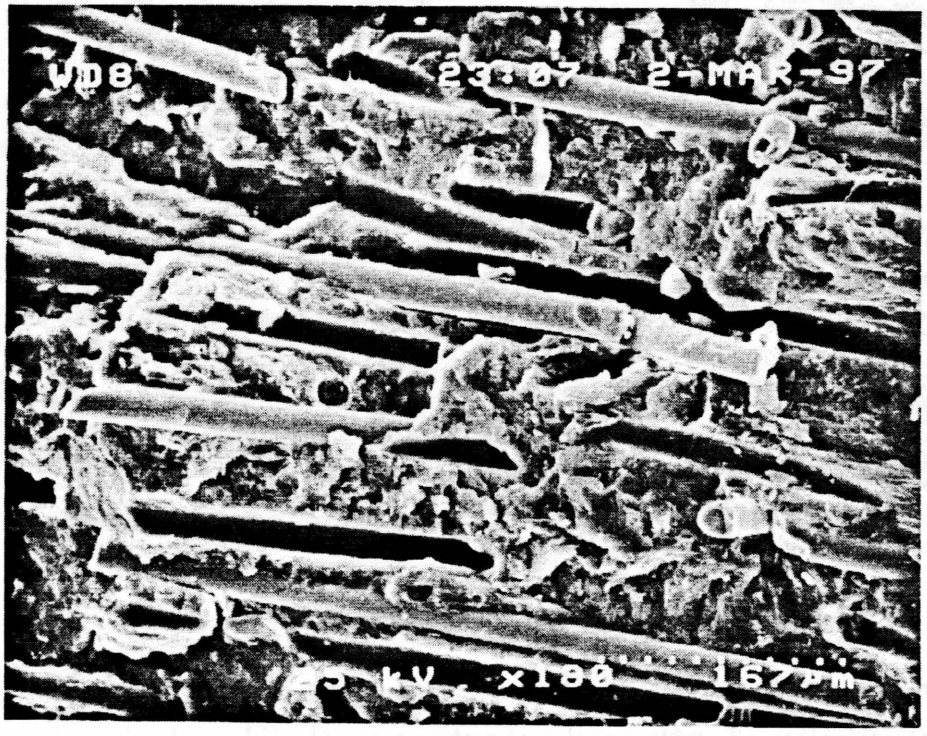

SEM 26 & 27 - RRT22 - Perpendicular (top) & Parallel - ~6mm - The fibers at this depth are dispersed evenly throughout the matrix and are oriented indicating an obvious flow direction.

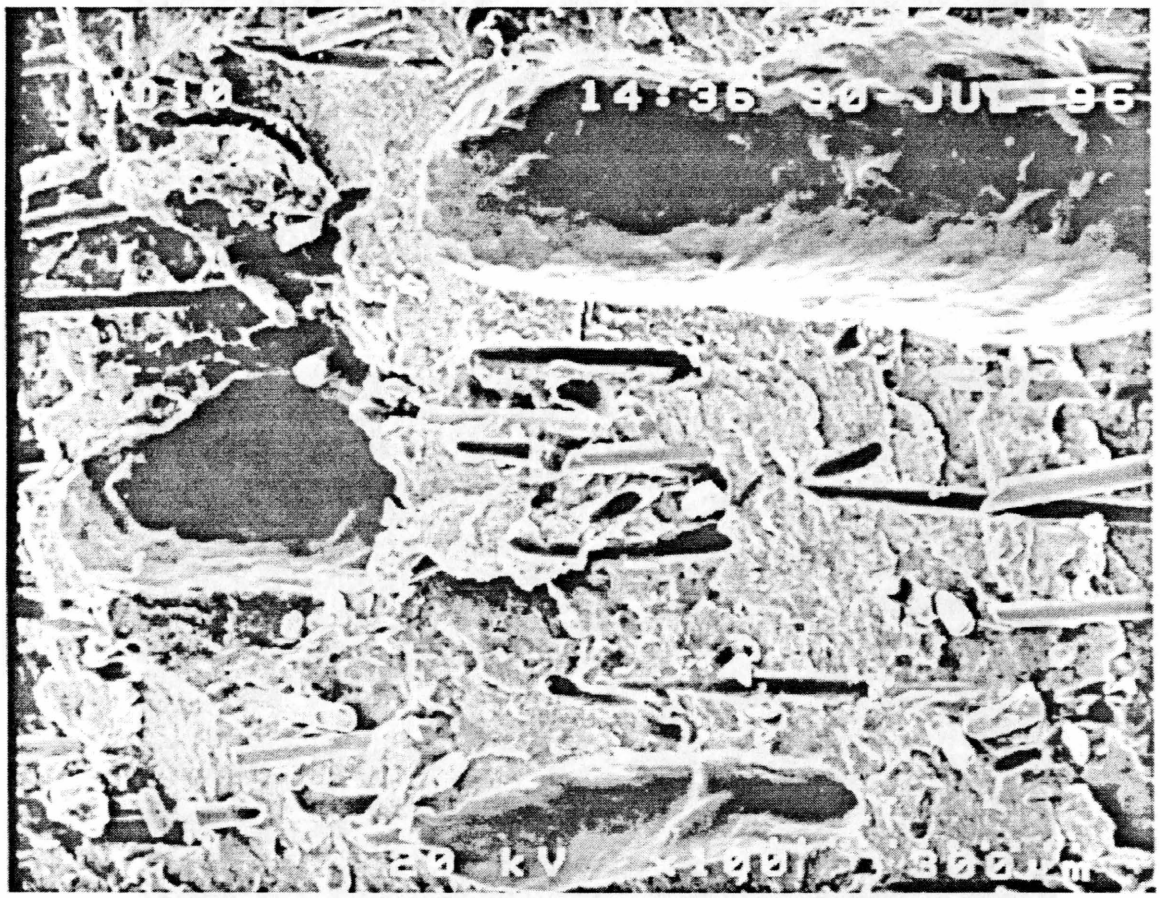

SEM 28 - RRT22 - Parallel - 18.6 - 25.4 mm - Voids in the matrix become larger at this depth and interfere with fiber behavior. There are no fibers within the holes, and fibers alignment is less consistent

28). The break down of fiber orientation and dispersion appears simultaneously with the appearance of large voids.

The fibers extend from the matrix in the same manner as the previous samples. The protruding fibers vary in length from 50 - 300 microns. There is almost no whetting of fibers with polymer. At increased depths, some adhesion occurs between PP and glass fibers, but this is uncommon. Near fibers, polypropylene is more common (SEM 29). In the parallel direction, long channels occur where fibers have pulled out of the matrix.

The relationship between PE and PP is similar to that of RRT28. Polypropylene is more abundant than observed in RRTUN, and it generally does not mix with PE. The two phases occur in streams that have definite borders between the two polymers (SEM 30).

SEM Conclusions:

The above observations tell us much about the relative strength and rigidity of the materials, as well as the degree of effectiveness enjoyed by the addition of reinforcing and coupling agents. Glass fibers add rigidity to the polymer, but to what degree is dependant on factors like dispersion and orientation. The excellent orientation of the fibers in these materials increases the ultimate tensile stress of the material. Much like steel-reinforced concrete, the glass fibers in the polymer will lessen the cracking effects of tensile stresses, because stress is transferred to the glass fibers. Homogeneous dispersion of glass fibers may lessen the effects of crack propagation. The rivets in ship hulls stop crack propagation in a similar manner. With fibers dispersed throughout the matrix, a crack is more likely to run into a fiber, which would stop the crack. The orientation and dispersion advantages apply most significantly to RRTUN. This material displays well-oriented fibers for the greatest range. The surface orientation for

SEM 29 - RRT22 - 6.2 - 12.4 m - The matrix near this fiber shows polypropylene loclized about the fiber with PE brdering PP.

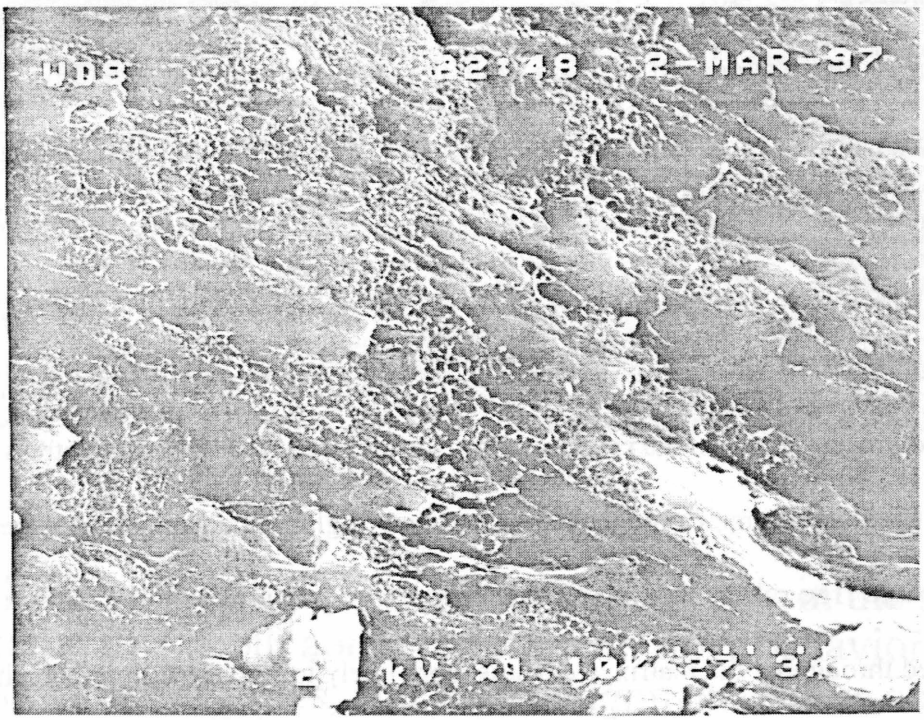

SEM 30 - RRT22 - Parallel - Surface - Two distinct phases of polymer, with elliptical dispersed phase PP oriented in the direction of flow.

RRT22 and RRT28 is poor, with RRT22 being the poorer of the two. Voids in the matrix of theses two materials appear at shallower depths, and occupy larger percentages of the matrix, which directly limits the effects of fiber orientation.

The volume fraction of the material that the fibers occupy also contributes to the material's relative strength. This calculation can be achieved by an area fraction method. A total number of six images in the perpendicular direction were collected and the total area of each section was calculated. Next, the total number of fibers and fiber holes is determined for each image. An average fiber diameter is determined by measuring four fiber diameters per window, and calculating the mean value. For these materials, the average fiber diameter was about 23 microns. The area fractions of glass fibers for this material RRTUN, RRT28, RRT22 are 3.65%, 3.08% and 3.67 respectively. This method for volume fraction is not highly accurate, so it is safe to state that each sample has about 3.5 % fibers with an error in the estimate of about 1%.

Although dispersion and orientation add to strength, their effects may be limited by the lack of fiber-matrix adhesion between the fiber and matrix. Glass fibers have a greater modulus than the polymer, and their function is to transfer some of the stress in the matrix to the stronger fiber. The lack of adhesion in all samples suggests that the fibers can just slide through the matrix when a certain stress is reached. The fracture mechanics inferred from SEM analysis suggests the same. The long, clean protruding fibers attest to the fact that failure occurs due to debonding of fibers from polymer. The matrix of the material begins to fail when cracks begin to form. When a crack reaches a fiber, the diverging sides of the crack cause tensile stress in the fiber causing short fibers to simply slide out of its existing encasement. If the fiber runs deep into the matrix, the fiber itself may crack. Crazing will also occur due to stress concentrations at

the fiber ends. If stress was truly transferred well from matrix to fiber, the ends of fibers would be covered with large clumps of polymer.

Polypropylene can shoulder two assignments. It can act as both a coupling agent and a reinforcing agent. The addition of polypropylene can increase the tensile strength and the modulus when it is mixed well with polyethylene. Elongation of dispersed phase polymer in the direction of flow suggests that polypropylene may help resist tensile forces parallel to the direction of flow. It will not, however, resist shearing stresses perpendicular to flow because the PP and PE are layered and have gaps at their borders. The nearly total isolation of the two phases in RRT22 and RRT28 will increase the likelihood of failure at the borders of the two phases. These observations lead the author to conclude that PP is acting as a poor reinforcing agent. Poor adhesion between the fiber and matrix also supports the conclusion that PP is not an effective coupling agent. Of the three samples, RRTUN enjoys the greatest support due to fiber reinforcement, but poor adhesion in all samples limits the possible structural advantage provided by the addition of glass fibers.

Mechanical Testing and Analysis

D.M.A. Sample Preparation:

Rectangular beams were cut from the bulk material with average dimensions of 20.00 mm x 3.25 mm x 1.25 mm. The long axis of the experimental samples were cut parallel to the long axis of the bulk beam. Stress ramps in three point bending were applied to these beams using a Perkin Elmer D.M.A.-7. Experiments of constant stress were also performed to determine creep strain values. All tests were performed at a constant temperature of 23.0 degrees Centigrade. The experiments of constant stress will here out be referred to as creep tests.

The previously described method of creating creep data from ramped data is applied to the composite polymer in question. Each material (RRT22, RRT28, RRTUN) is subjected to creep tests and ramped tests. Approximate values for creep strains are determined from ramped experiments and compared with experimental values for creep. Several samples were tested for each material.

A slow rate (1 mN/min) and a fast rate (500 mN/min) are applied to each sample. A slight complication with stress rates occurs, due to the varying cross sections of the samples, and the limitations of experimental equipment. The range of sample sizes causes varying fast rates from 2.7 MPa/min to 3.3 MPa/min, and varying slow rates from 5480 Pa/min to 11600 Pa/min. This makes it impossible to determine averages for fast and slow ramps strictly from experimental data.

One can resolve this dilemma through the application of equations 4 - 10. Values of m

for specific stress-strain products are determined between experimental fast and slow ramps for one sample. The experimenter can now approximate ramps at a fast rate (2.75 MPa/min) and slow rate (2778 Pa/min) for each sample. Once these ramps are created for a significant number of samples (for each material), fit-equations using fifth order polynomials[12] are created, and average ramps of stress and strain are created for fast and slow stress rates. From these average ramps, the author uses equations 4 - 10 again, to determine universal m values for each material. These m values are plotted against the corresponding values of stress-strain product. Using equation 3 to determine the necessary stress rate, the author can now create a ramp from which one can determine the approximate creep strain at the necessary time.

In addition to ramp experiments, creep tests were performed by applying a constant stress to various samples for a period of time. The experimental creep stress is 1.5 MPa applied for a period of 300 minutes. The data from these experiments is employed for direct comparison to the results achieved from the approximate method in Table 1.

Multiple fast and slow ramps were run until a set of samples is chosen that corresponds to the behavior of the major portion of the material. From these ramps, three were chosen for each rate and material. Analysis is performed on these ramps. For creep curves, an average of several curves for each material is used for comparative purposes.

In determining values for the exponent m and its relationship to the stress strain product

---

[12]For several samples third order polynomials were used to provide superior approximations.

Material	RRT22	RRT28	RRTUN
experimental strain (%)	.209834	.140657	.149224
calculated strain (%)	.185099	.139103	.1451164
% error	13.36%	1.1%	2.8%

Table 1 - This table displays the relationship between the experimental creep strains and the calculated creep strains for each material tested.

($\sigma\epsilon$), the experimenter may notice significant variation in the m values and in the shape of the m vs. $\sigma\epsilon$ product curve. The values of m at low $\sigma\epsilon$ can be neglected, because this portion of the curve represents the effects of the instantaneous loading of the material. The values of m generally converge toward a certain value for a sample. This value may vary from sample to sample due to the variations in the morphology of different samples. Although the m values may differ significantly, (as much as 35%), this will not have a significant effect on the approximated curves for one material.

To elucidate this fact, m vs. $\sigma\epsilon$ curves of material RRTUN, for the three samples selected for analysis, are displayed (Curve 1, 2, 3). Between the $\sigma\epsilon$ values of .2 million and 1.2 million, the m values for sample 11 range from .0338 to .0353, for sample 8 from .0488 to .0467, and for sample 7 from .0263 to .0316. This variation appears significant, but when these values are used to create stress-strain ramps, only slight variation occurs. This is evident in Curve 4 where slow and fast ramps at the same rate were created from the m values for the fore mentioned samples. The black lines represent the averages of the three fast and slow curves. These averages are used to determine a universal m vs. relationship for material RRTUN. This m relationship is shown in Curve 5. Using these values, one can create a ramped curve at any stress rate, and determine stress, strain and time.

This method was performed on materials RRT22 and RRT28 with similar results. A plot of slow and fast ramps with averages is provided for each material (Curve 6, 7). Plots of the universal m values vs. $\sigma\epsilon$ is also included for each material (Curve 8, 9). These values were

used to create ramps at a stress rate of 5000 Pa/min. This rate was determined using the creep/ramps relationship for a creep experiment with 1.5 MPa applied for 300 min. For comparison between materials, ramps at this rate for each material are plotted on the same graph (Curve 10). One can see that RRTUN and RRT28 have similar curves, while RRT22 displays significantly less resistance to deflection under comparable stress for the same time interval.

These curves are superimposed with the actual creep experiments for the three materials (Curve 11). The creep curves provided are averages of several creep tests for each material. The behavior indicated by the ramps is similar to that observed under creep testing. RRT28 and RRTUN display a greater resistance to creep than material RRT22.

The difference between the points on the creep curve and ramped curve, for each material, represents the error in the approximation. If this was an exact method, the two curves (ramped and creep) would meet exactly at 300 minutes. The values for actual and experimental creep strains vary by an average of only 5.7 %. The greatest variation of 13.5 % occurs in material RRT22, while material RRT28 only varies by 1.1 %. Since this method is applicable on the short term, we can expand the analysis to predict creep strains for long periods of time. If we use a time of 25 years for an example, we can determine a rate for this time and create a ramp to render the creep strains at 25 years for each material. Curves for each material are provided on Curves 12, 13, 14.

Conclusion:

We can draw several conclusions from the relationship between the morphological

characteristics and the mechanical properties of these materials. RRTUN displays the most consistent fiber behavior for the greatest range. RRTUN also has the greatest resistance to creep. This indicates that the glass fibers provide resistance to creep deformation. It is also known that a pure polymer will creep significantly more than a fiber-reinforced polymer.

All three materials have morphological properties that are very similar, but one material, RRT22 creeps slightly more than the other two materials. A source of this discrepancy may be the fact that mechanical testing was performed only on small sections taken near the outer surface of the material. Since RRT22 displays the poorest surface orientation of fibers, and the samples were taken near the surface, the tests on this material may only indicate the behavior of the surface. If samples were taken from various depths, where morphological characteristics are known, a better representation of the material's mechanical properties may be achieved.

The interaction between fiber and matrix is an important factor in reinforcement. When comparing SEM 4 to SEM 9, we can see that polypropylene provides some coupling between glass fiber and matrix. In figure 4 where only glass fiber and PE occur, significant gaps between fiber and matrix occur. These gaps are more significant than those in the PE/PP composite. However, the material could achieve superior strength with a coupling agent that creates a fiber matrix relationship comparable to that of SEM 3.

The important conclusion from this analysis is the agreement between the experimental and calculated creep strains. The effectiveness of this method for glass fiber reinforced composites allows us to expand this analysis to any polymeric material which behaves in a

similar mechanical fashion.

The ability to predict the long term mechanical properties for polymeric composites will undoubtedly expand the realm of applications for polymeric materials. An engineer will always be reluctant to use an unproven material in a structure where lives are at risk. Accurately predicting long term effects on these materials may encourage more engineers to place trust in polymers for structures. Only with predictive methods like this and time will the polymer industry expand to reach its full potential.

Suggestions For Future Work

As mentioned previously, a source of error in mechanical testing may be the location of sample extraction from the bulk beam. One way of avoiding this error is testing of the entire beam. This will provide complete characterization of the beam without concern for variations in morphology. If the means for large scale testing are not available, SEM prior to D.M.A. sample extraction will avoid this error. If a complete SEM study of the entire material is performed, the experimenter will know where the strong and weak points in the material exist, enabling one to extract samples of known morphology.

Since the polymer composite in question is to be used as a railroad tie, perhaps creep is not the proper study to perform. Railroad ties are not subject to a sustained dead load, but dynamic live loads, fatigue analysis would be useful. The use of dynamic mechanical testing can better simulate the loads applied by trains. As mentioned previously, the addition of a more

effective coupling agent or a higher percentage of glass fibers are both pre-molding techniques for strengthening the material. All of these methods are dependent on cost and the relationship between current properties and the accepted specifications for railroad ties.

m vs sigma*epsilon

RRTUN plo7

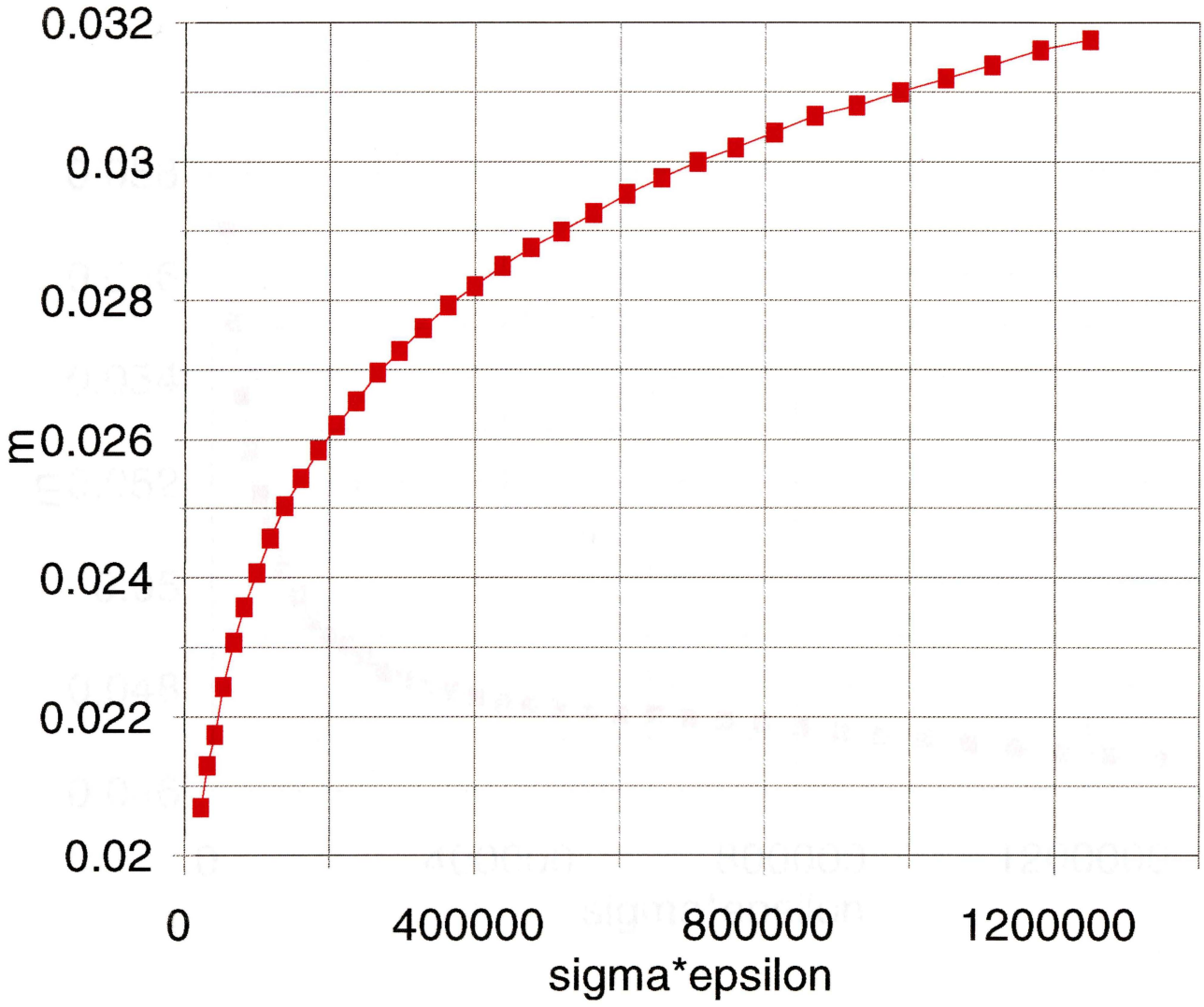

Curve 1, 2, 3 display the different shapes of the m vs stress-strain product for different samples of the same material, RRTUN. This variation will not significanly affect the calculated creep strains.

m vs sigma*epsilon

RRTUN plo8

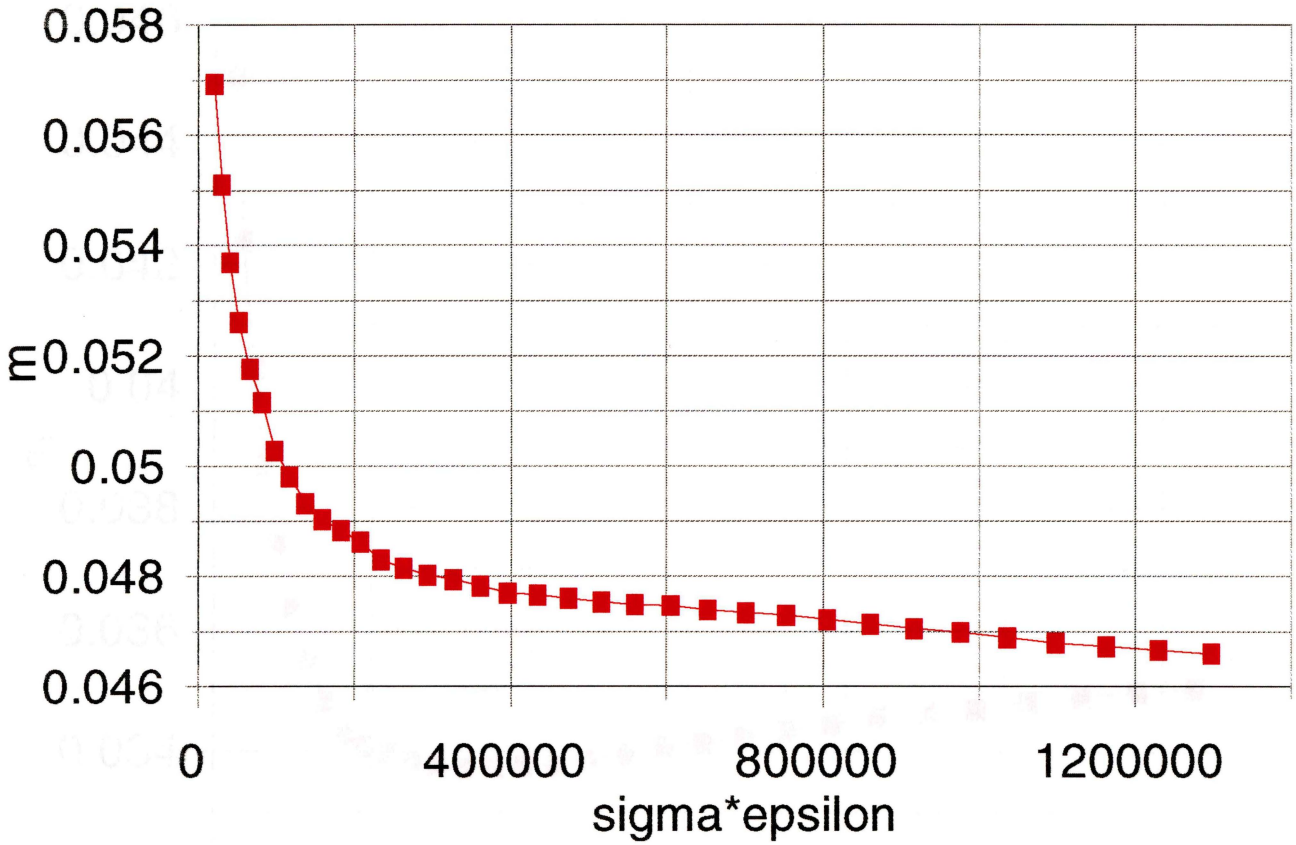

Curve 2

m vs sigma*epsilon

RRTUN plo11

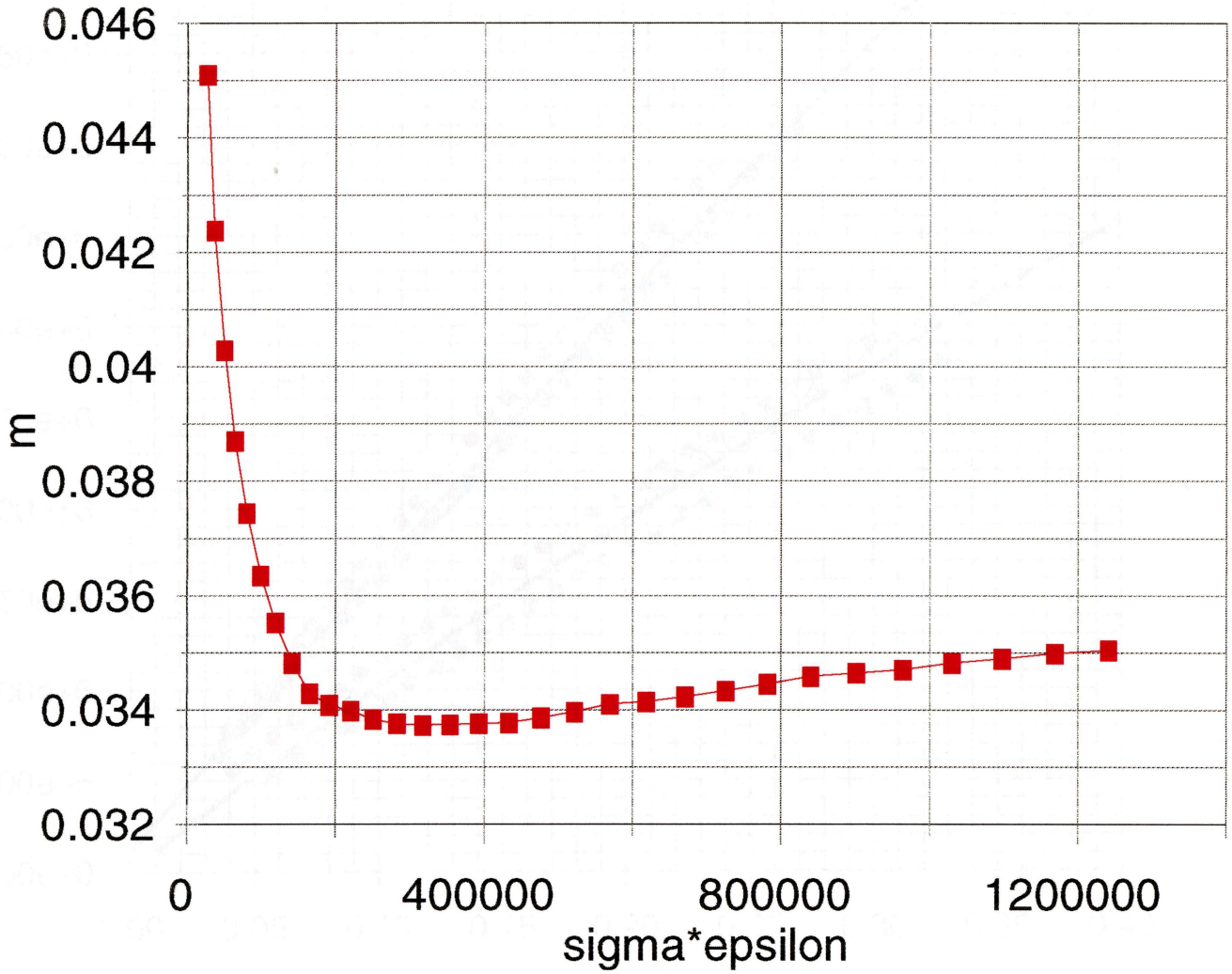

Curve 3

RRTUN - Fast and Slow Ramps

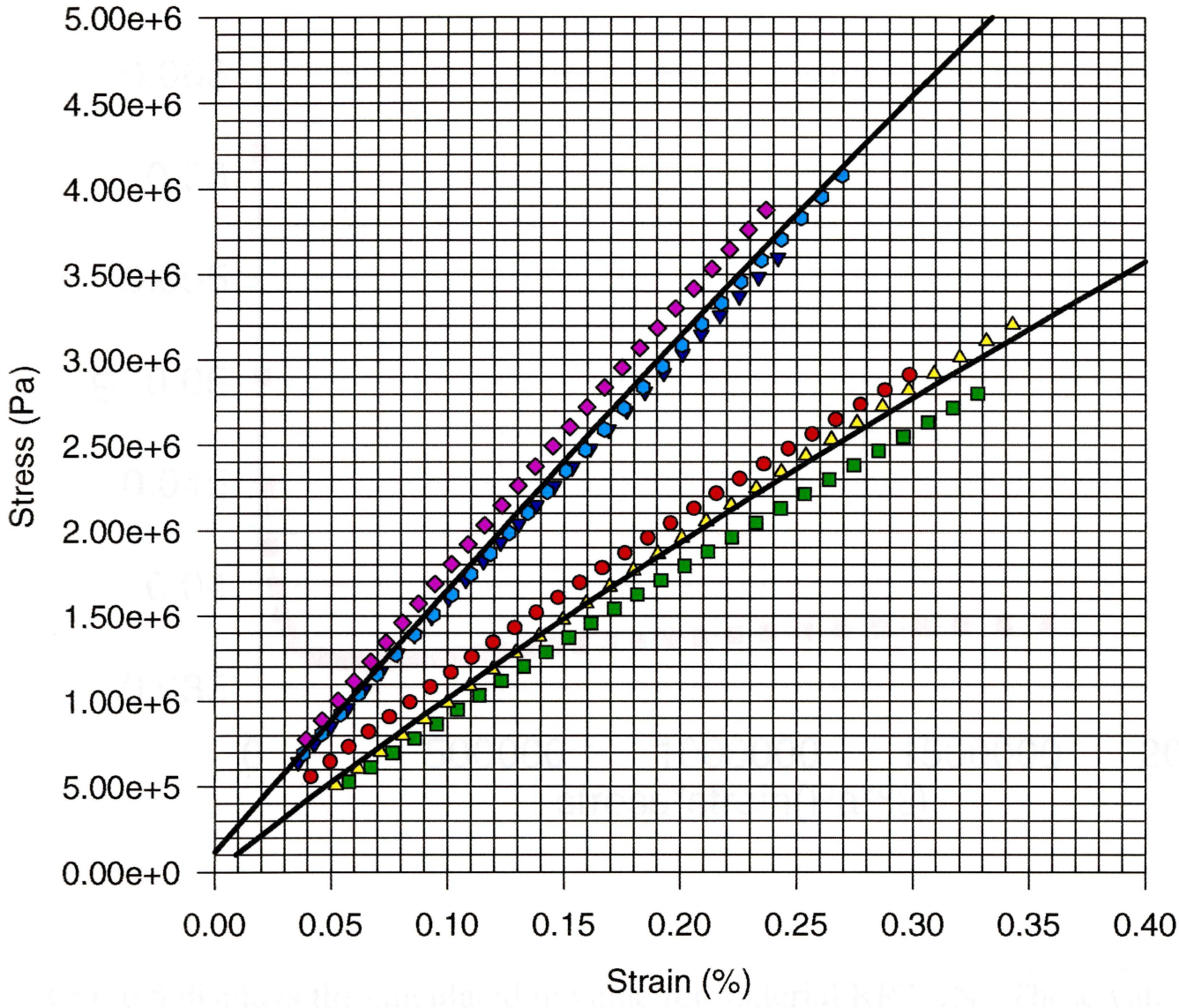

Curve 4 displays the calculated stress-strain curves at the slow and fast rates for material RRTUN. The black lines represent the average of the slow and fast curves

m vs sigma*epsilon

RRTUN - Final

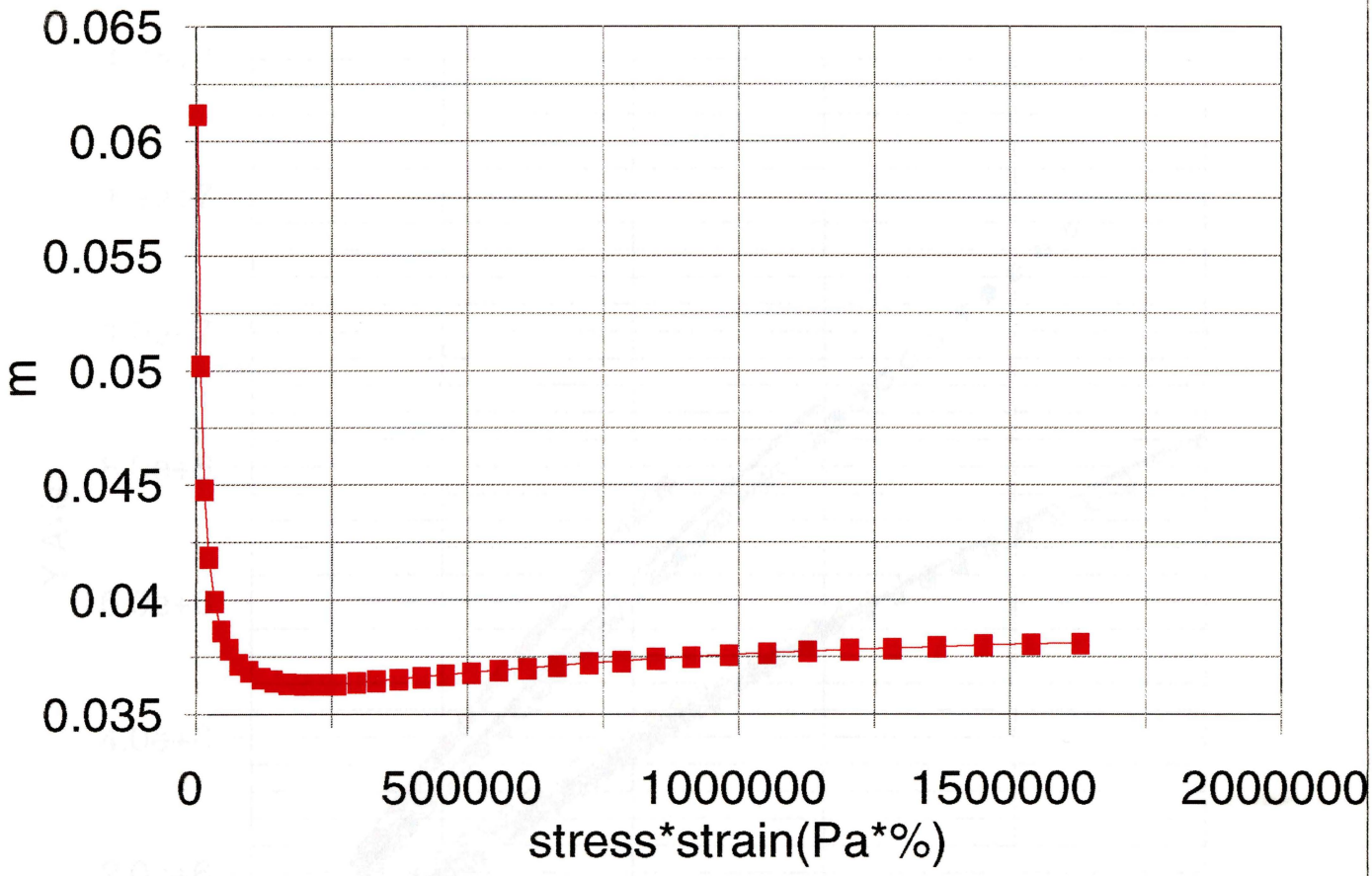

Curve 5 displays the calculated m value for material RRTUN. These values can be used for any ramp stress and strain calculation for this material.

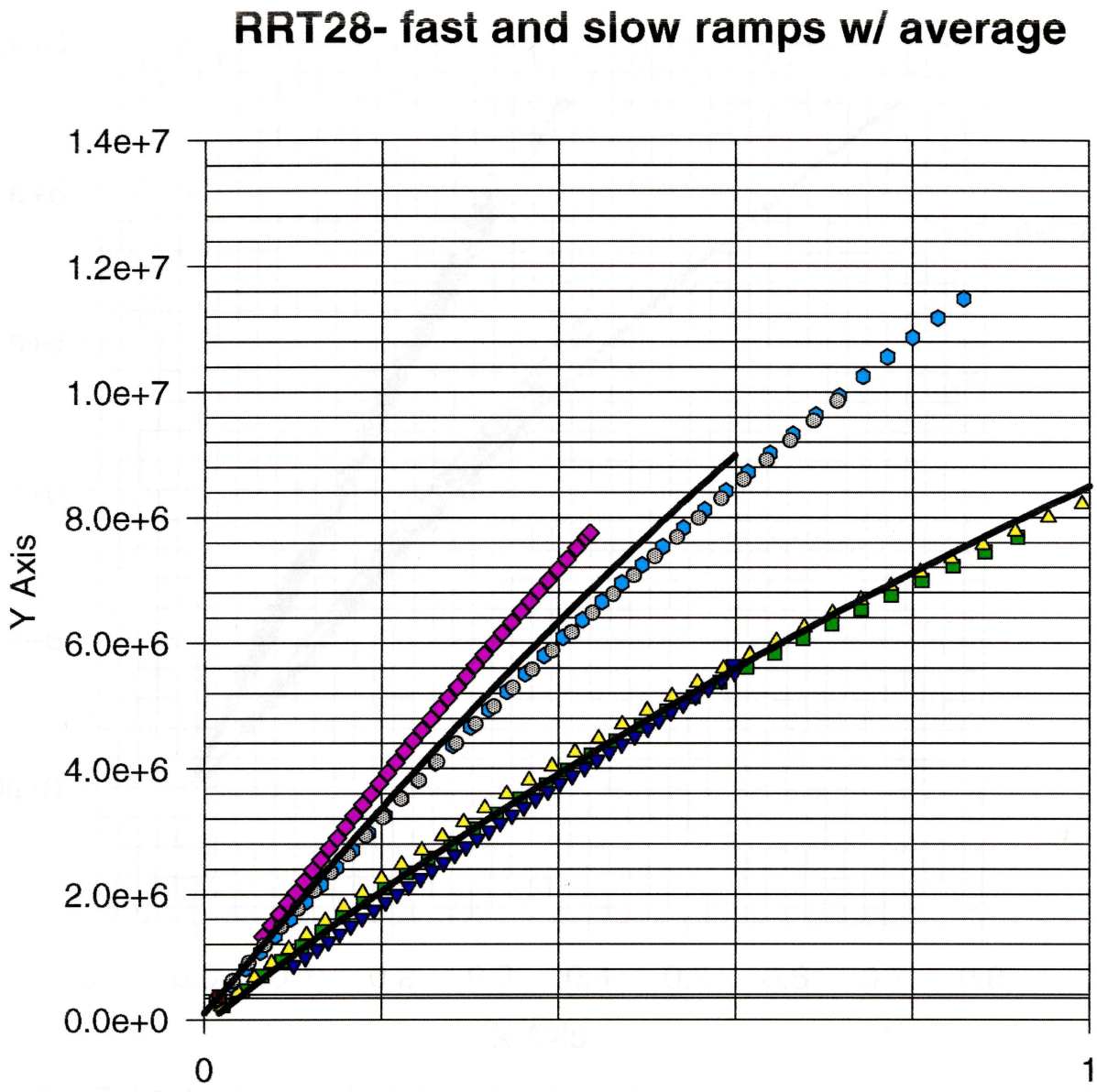

Curve 6 displays the calculated stress-strain ramps at the fast and slow rates for material RRT28. The black lines represent the average of each of the three curves

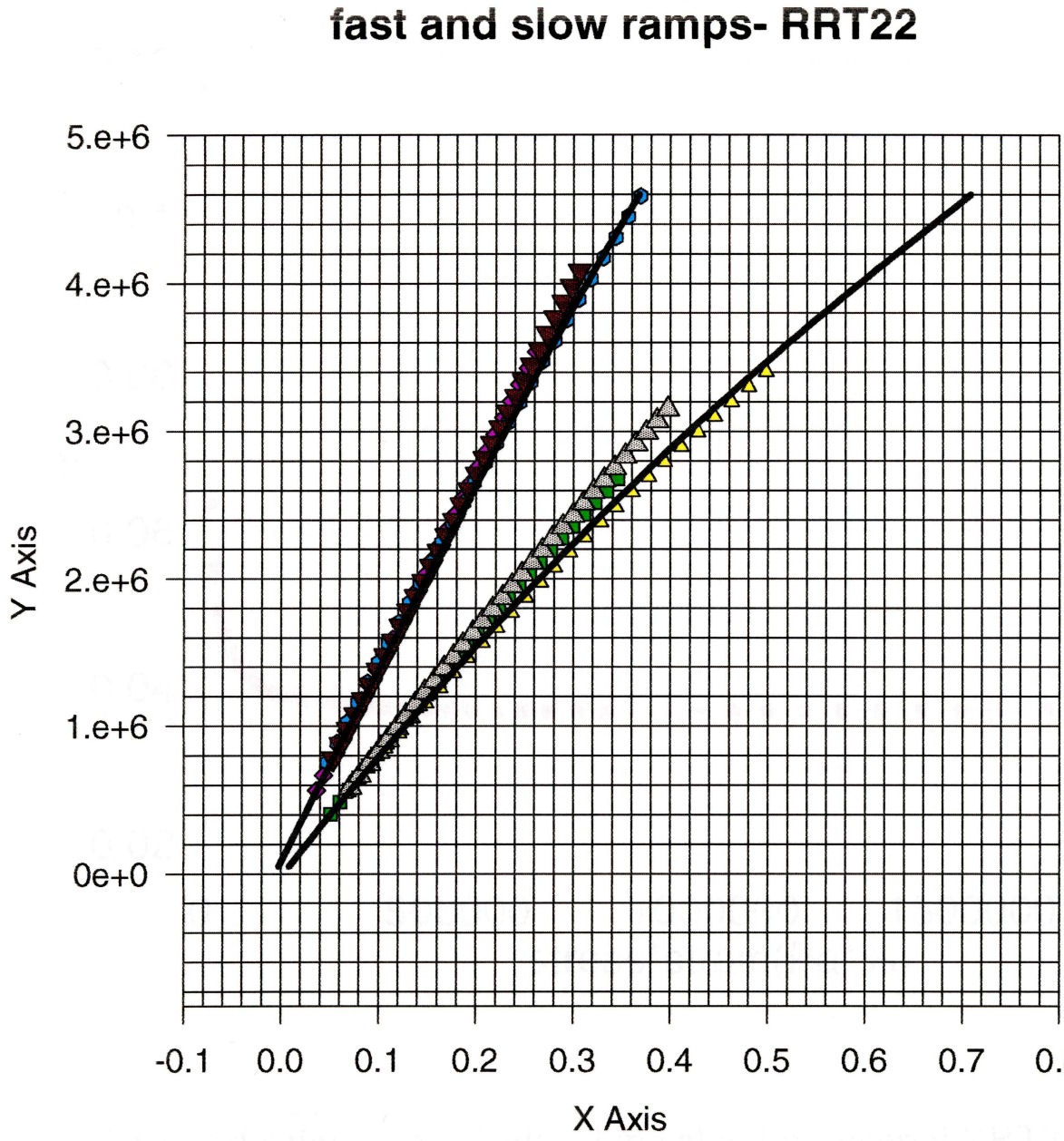

Curve 7 displays the calculated stress-strain ramps at the slow and fast rates for material RRT22. The black lines represent the average of the slow and fast curves

m vs sigma*epsilon

RRT28 - Final

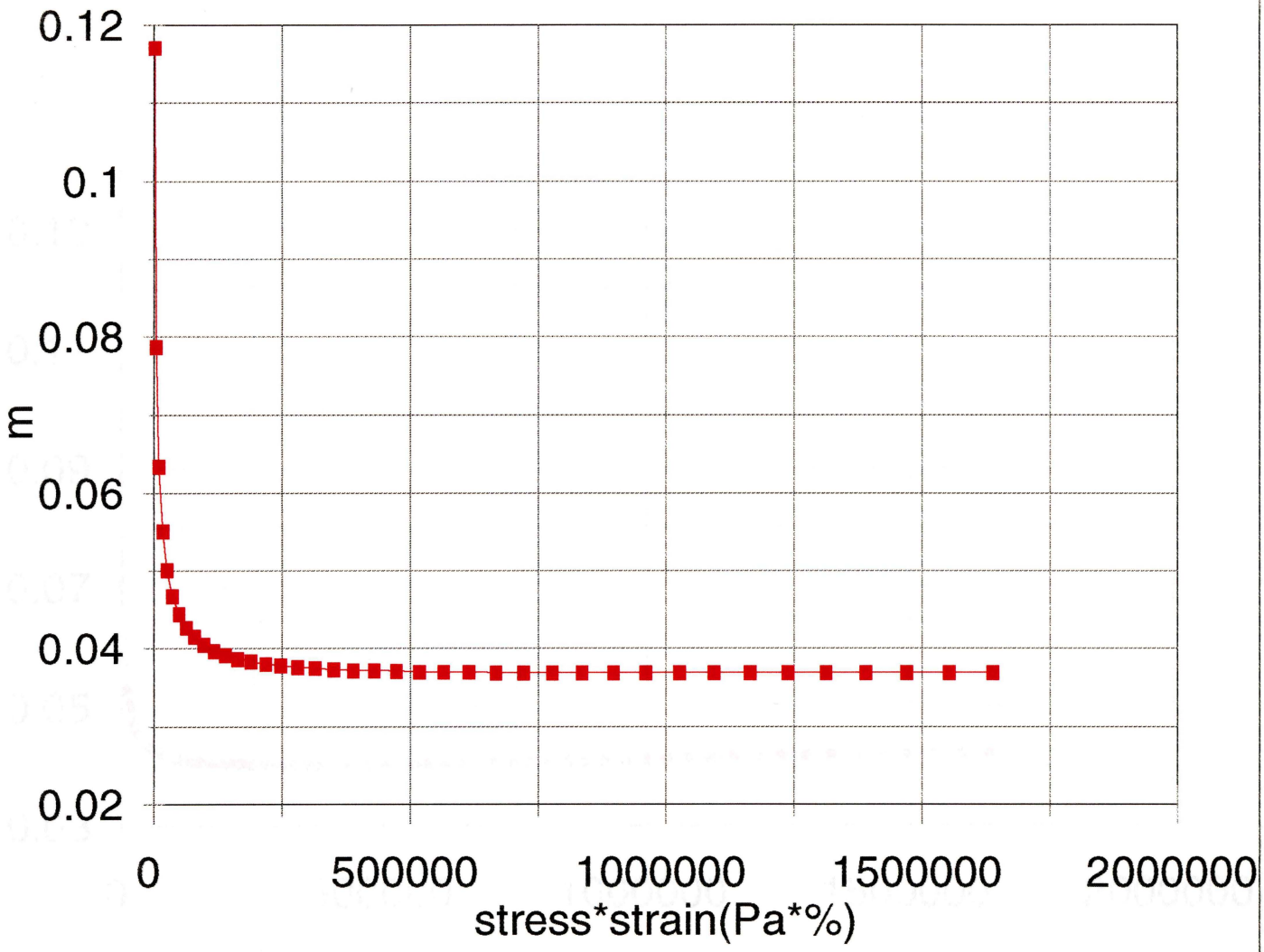

Curve 8 displays the calculated m value for material RRT28. These values can be used for any ramp stress and strain calculation for this material.

m vs sigma*epsilon

RRT22-FINAL

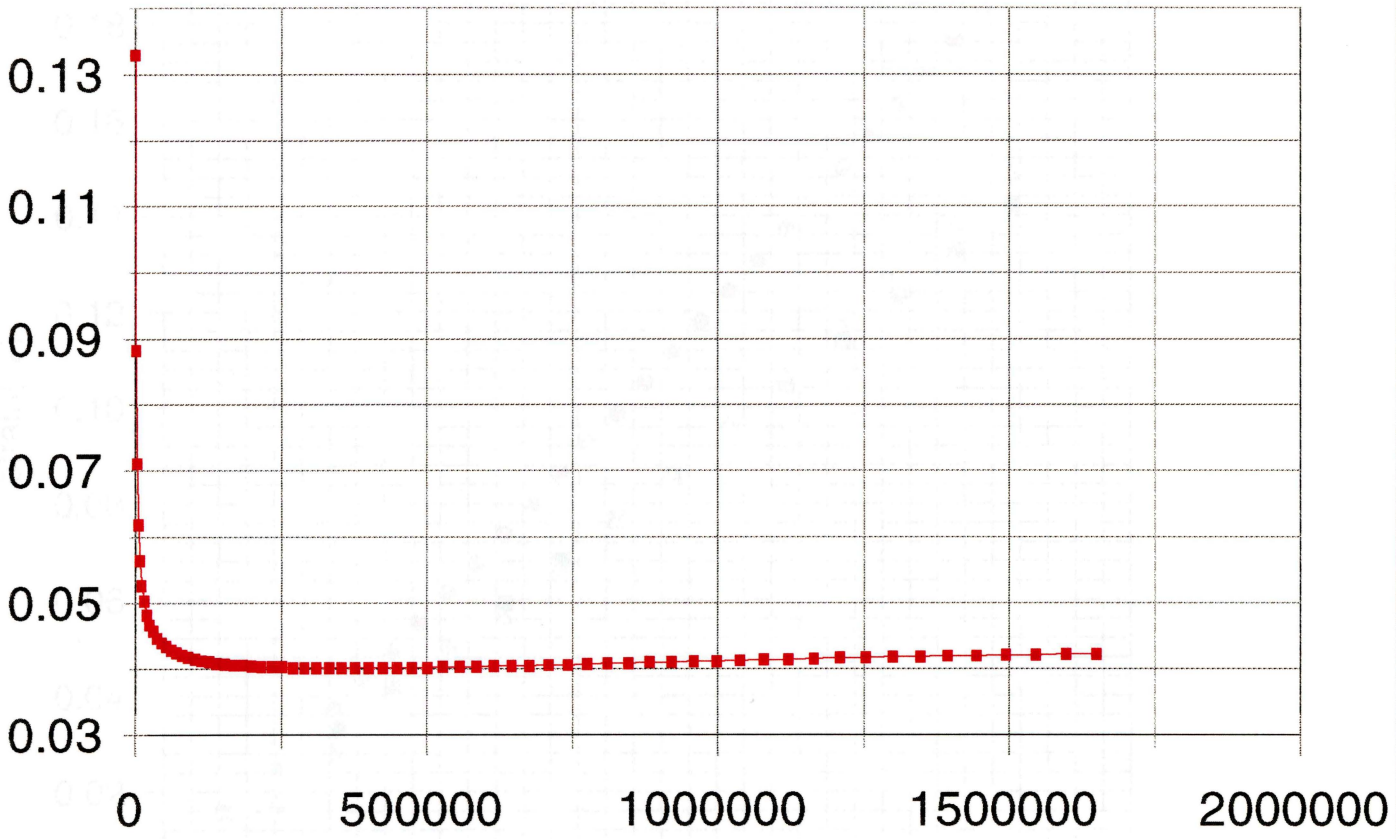

Curve 9 displays the calculated m value for material RRT22. These values can be used for any ramp stress and strain calculation for this material.

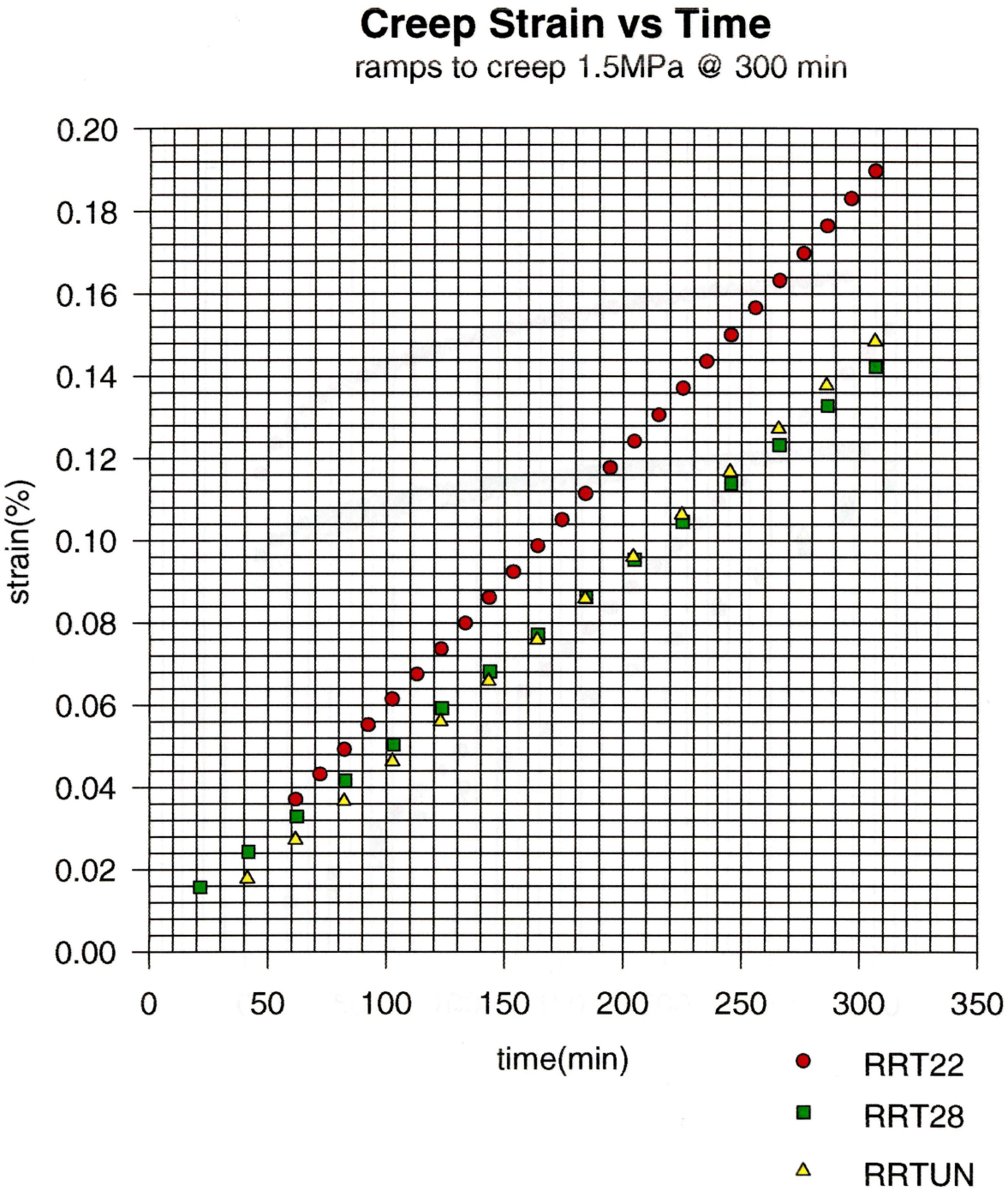

Curve 10 displays the calculated creep ramps for 1.5 MPa for 300 minutes for each of the three materials

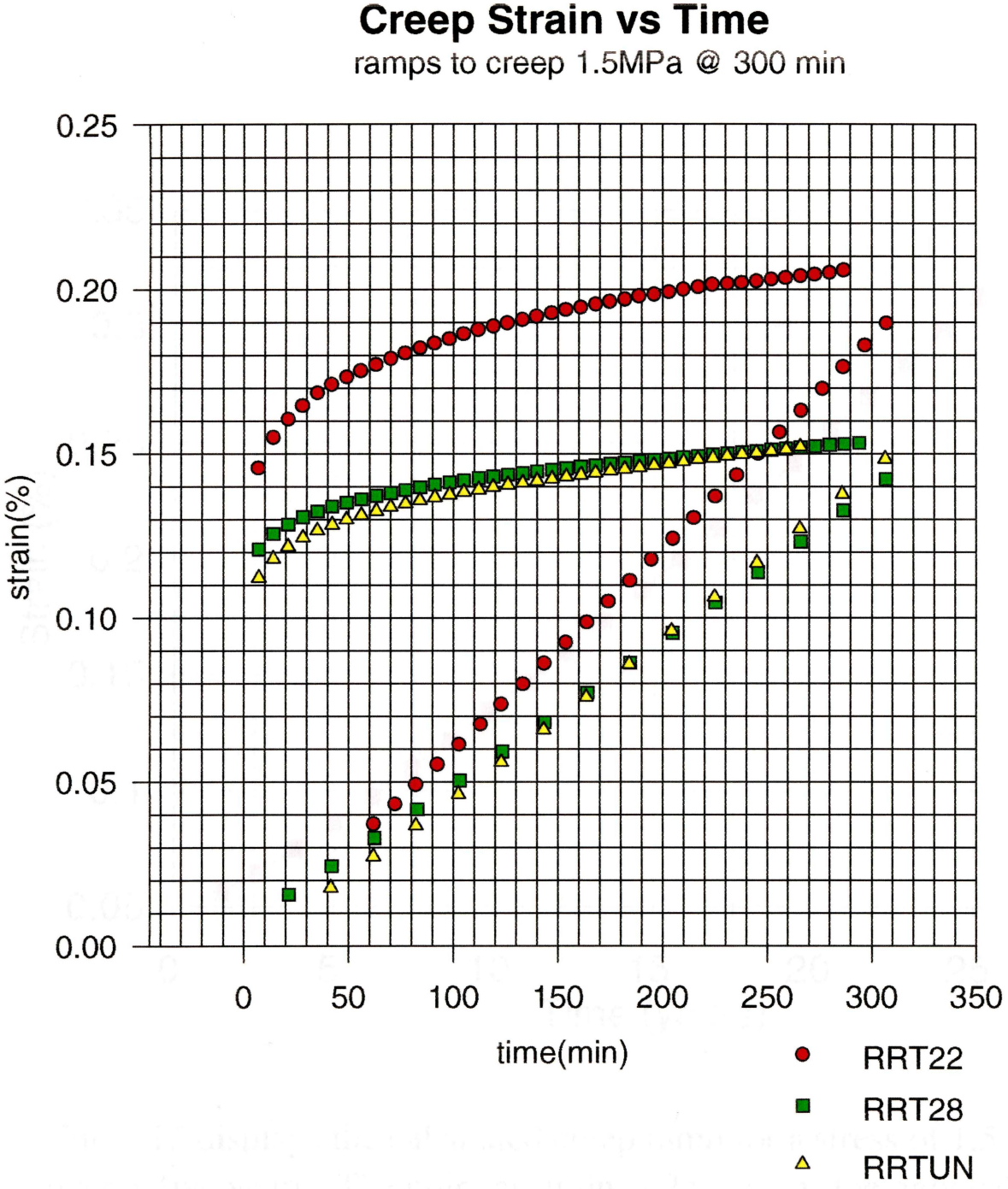

Curve 11 shows the relationship between calculated creep ramps and experimental creep tests for each material. If this method was exact, the two curves would meet at 300 minutes

Strain vs Time .1142 Pa/min

RRT28 creep ramp for 1.5 MPa @ 25 yrs

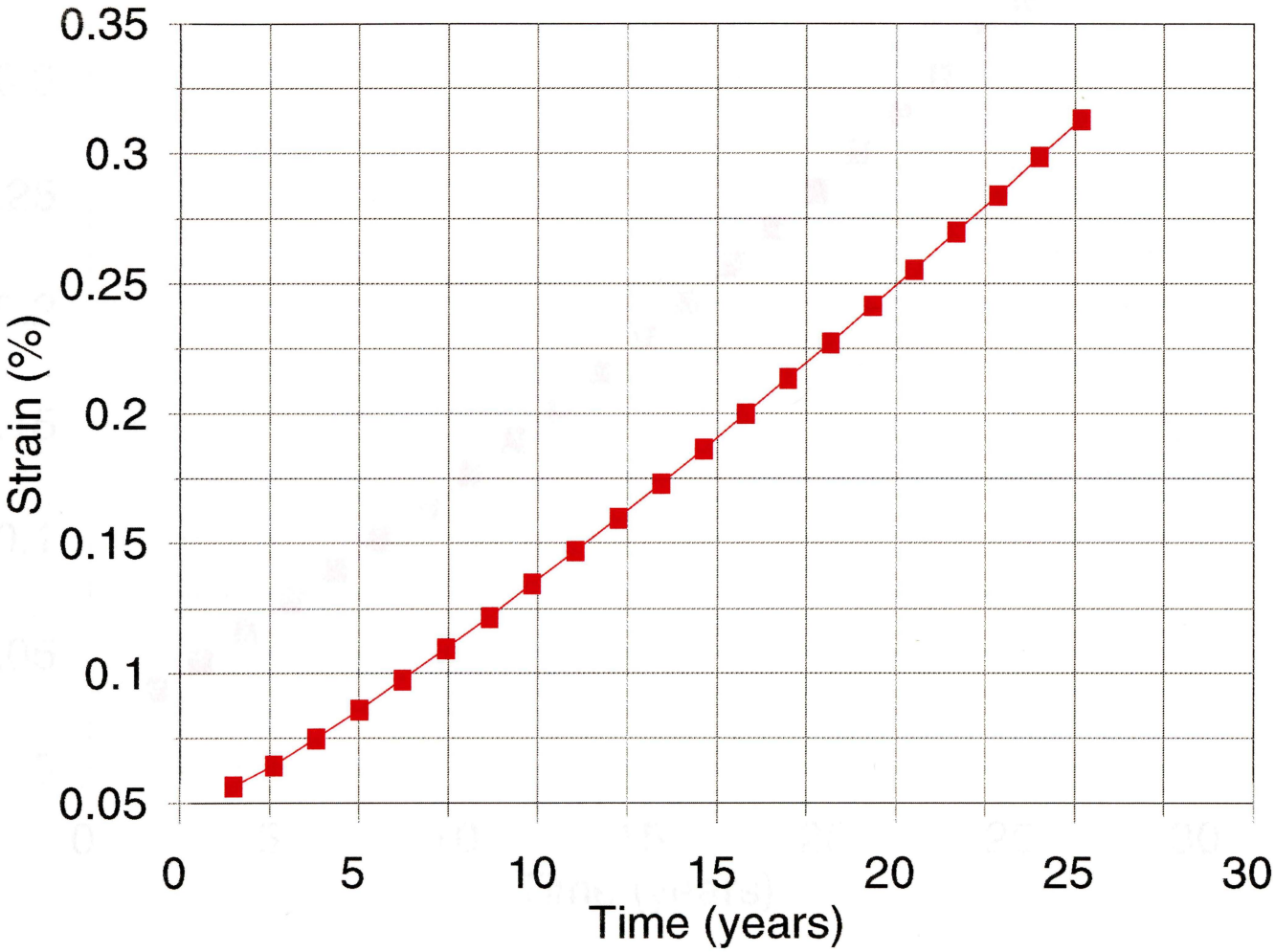

Curve 12 displays the calculated creep ramp for a stress of 1.5 MPa at twenty five years. The point at strain at 25 years is the only valid strain to be considered.

Strain vs Time .1142 Pa/min

RRTUN creep ramps for 1.5 MPa @ 25 yrs

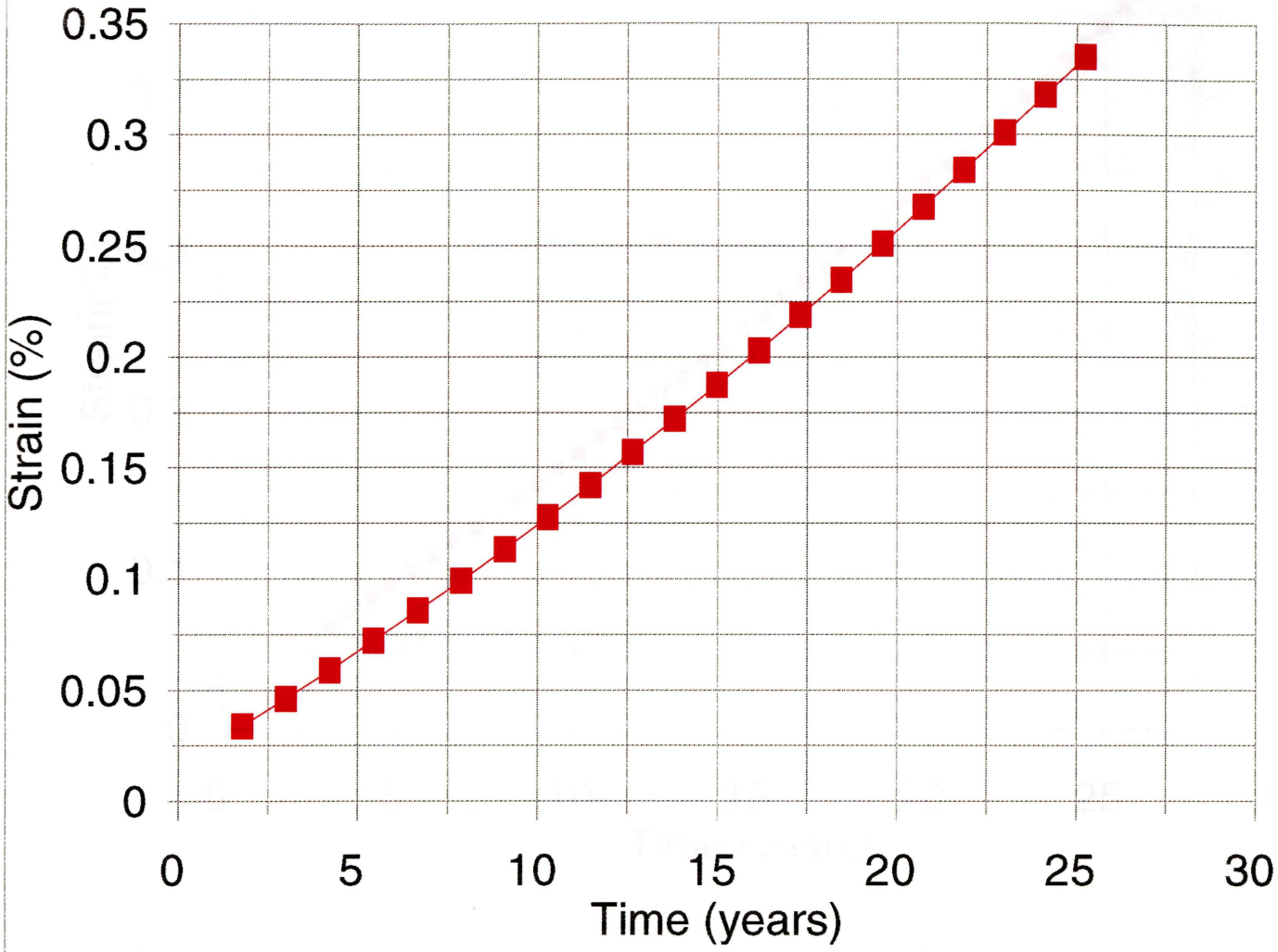

Curve 13 displays the calculated creep ramp for RRTUN at a stress of 1.5 MPa at a time of 25 years.

Strain vs Time .1142 Pa/min

RRT22 creep ramp for 1.5 MPa @ 25 yrs

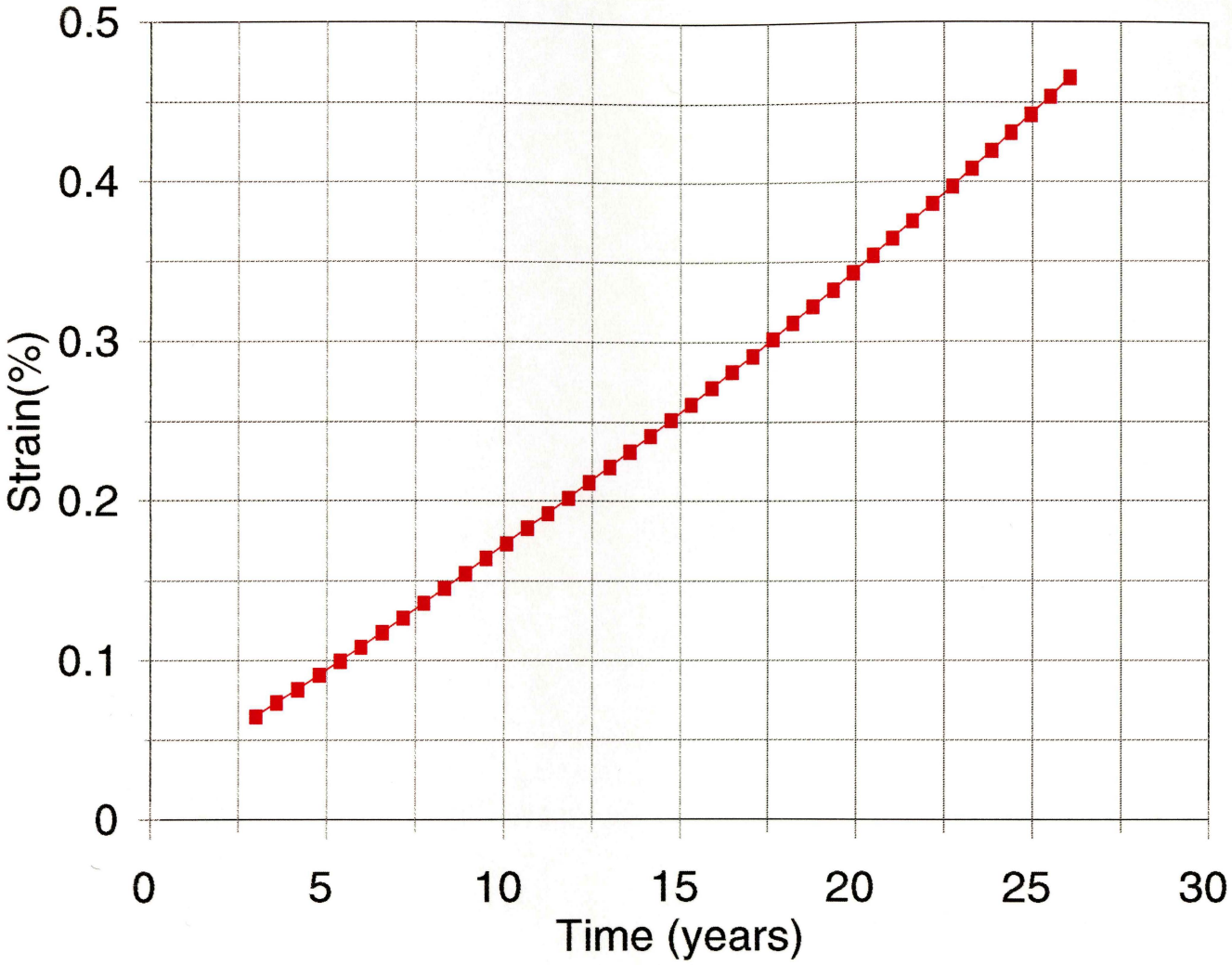

Curve 14 displays the calculated creep ramp for a stress of 1.5 MPa for 25 years.